iScience

CellPress
OPEN ACCESS

Article

RPRM negatively regulates ATM levels through its nuclear translocation on irradiation mediated by CDK4/6 and IPO11

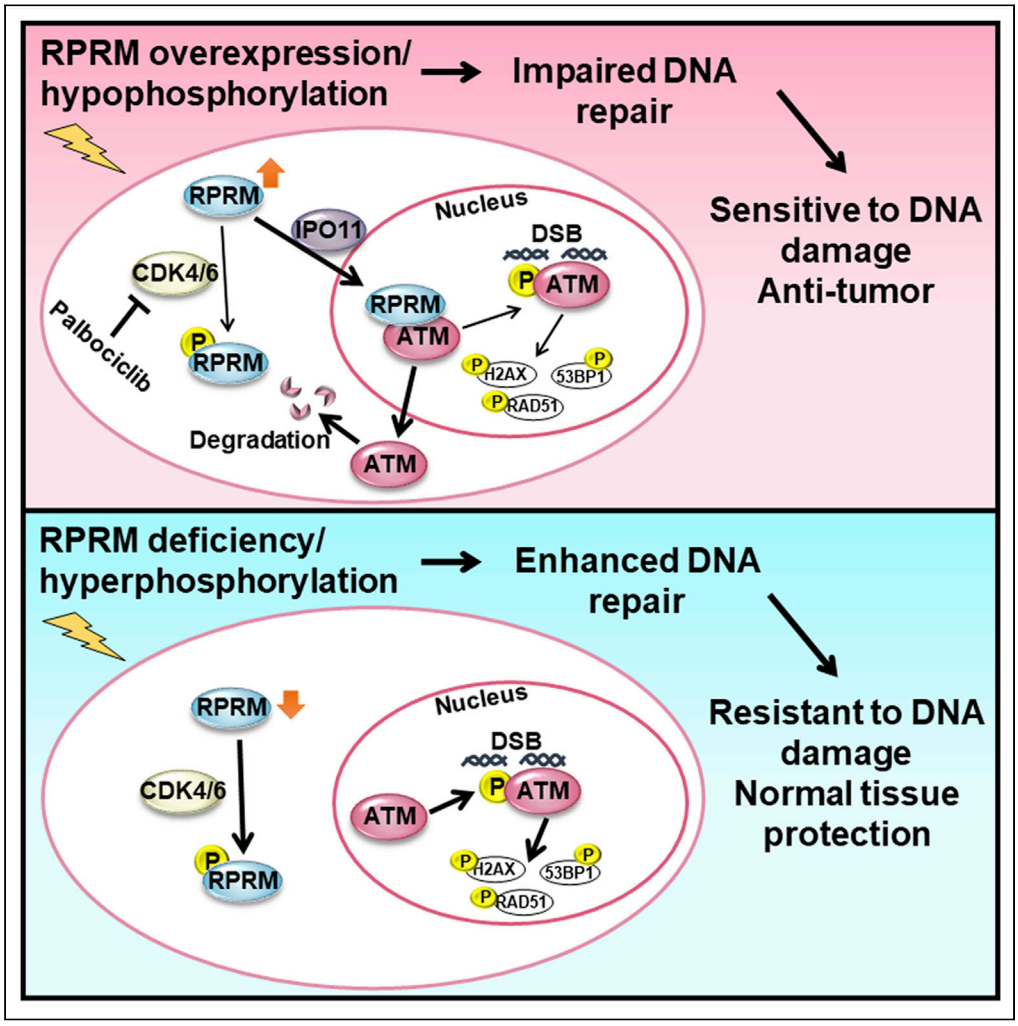

Yarui Zhang, Guomin Ou, Zhujing Ye, ..., Jingdong Wang, Jianping Cao, Hongying Yang

yanghongying@suda.edu.cn

Highlights

RPRM negatively regulates ATM, thus determining cellular sensitivity to DNA damage

On nuclear import, RPRM binds to ATM, promotes ATM nuclear export and degradation

RPRM nuclear import is governed by its phosphorylation status mediated by CDK4/6

IPO11 is essential to the nuclear translocation of RPRM on induction

Zhang et al., iScience *25*, 105115
October 21, 2022
https://doi.org/10.1016/j.isci.2022.105115

iScience

CellPress
OPEN ACCESS

Article

RPRM negatively regulates ATM levels through its nuclear translocation on irradiation mediated by CDK4/6 and IPO11

Yarui Zhang,[1,3] Guomin Ou,[2,3] Zhujing Ye,[1] Zhou Zhou,[1] Qianlin Cao,[1] Mengting Li,[1] Jingdong Wang,[1] Jianping Cao,[1] and Hongying Yang[1,4,*]

SUMMARY

How the ataxia telangiectasia mutated (ATM) protein kinase, a core protein in DNA damage response, is regulated at post-transcription level remains unclear. Here it is identified that protein Reprimo (RPRM) downregulates ATM protein levels, resulting in impaired DNA repair and enhanced cellular radiosensitivity. Mechanistically, although primarily localized in the cytoplasm, RPRM translocates to the nucleus shortly after induced by X-irradiation, interacts with ATM and promotes its nuclear export and proteasomal degradation. The RPRM nuclear translocation involves its phosphorylation at serine 98 mediated by cyclin-dependent kinases 4/6 (CDK4/6), and requires Importin-11 (IPO11). Of importance, IPO11-regulated RPRM nuclear import upon irradiation is essential for its regulation on ATM. Thus, RPRM overexpression and its phosphorylation inhibition sensitize cells to genotoxic agents such as irradiation, whereas RPRM deficiency significantly increases resistance to radiation-induced damage both *in vitro* and *in vivo*. These findings establish a crucial regulatory mechanism in which ATM is negatively modulated by RPRM.

INTRODUCTION

The ataxia telangiectasia mutated (ATM) protein kinase, a member of the phosphatidylinositol-3-OH-kinase (PI(3)K) family, is a master regulator of DNA damage response (DDR) in the presence of double-strand breaks (DSBs), which determines DNA repair efficiency and cellular sensitivity to DSBs, thus playing critical roles in genomic stability, cell death, survival, etc. (Marechal and Zou, 2013; Shiloh, 2003; Kastan and Lim, 2000; Shiloh and Ziv, 2013). Mechanistically, upon DSB induction in mammalian cells, the intermolecular autophosphorylation and monomerization of ATM occur rapidly, leading to its activation (Bakkenist and Kastan, 2003; Berkovich et al., 2007). ATM is also recruited to DSB sites and activated by MRE11-RAD50-NBS1 (MRN) complex (Lee and Paull, 2004). Activated ATM then phosphorylates its thousands of downstream DDR-related proteins, such as H2AX, 53BP1, P53, CHK2, etc., thus setting an intricate and fine-tuned DDR network to repair damaged DNA (Kastan and Lim, 2000; Shiloh and Ziv, 2013; Matsuoka et al., 2007; Bensimon et al., 2010). Therefore, ATM deficiency or defects lead to enhanced cellular sensitivity to genotoxic agents. A typical example is ataxia telangiectasia (A-T), an autosomal recessive disease caused by mutations in the ATM gene (Savitsky et al., 1995). Thus, A-T patients exhibit hypersensitivity to ionizing radiation (IR) in addition to a wide range of symptoms including neurodegeneration, senescence, immunodeficiency and cancer susceptibility (Anheim et al., 2012; Spacey et al., 2000; Perlman et al., 2012; Lavin, 2008). In addition, ATM is considered as an effective and sought-after target for cancer therapy. Its two highly selective inhibitors, AZD0156 (Riches et al., 2019) and AZD1390 (Durant et al., 2018), have entered phase I cancer clinical trials (Jin and Oh, 2019). There have been extensive studies on how ATM regulates its various downstream targets of DDR and the underlying mechanisms (Kastan and Lim, 2000; Shiloh and Ziv, 2013; Matsuoka et al., 2007; Bensimon et al., 2010), but how ATM itself is regulated immediately after DSB induction is still not fully understood.

Reprimo (RPRM), a single-exon (intronless) 327-bp gene that is located at 2q23, encodes a highly glycosylated protein (Ohki et al., 2000). RPRM is believed to be a tumor suppressor gene (Amigo et al., 2018). Its downregulation because of aberrant methylation of its promoter has been found in a variety of cancers such as breast (Buchegger et al., 2017), gastric (Ooki et al., 2013), pituitary (Xu et al., 2012), and pancreatic

[1]State Key Laboratory of Radiation Medicine and Protection, School of Radiation Medicine and Protection, Suzhou Medical College of Soochow University/Collaborative Innovation Center of Radiation Medicine of Jiangsu Higher Education Institutions, 199 Renai Road, Suzhou Industrial Park, Suzhou, Jiangsu Province 215123, P. R. China

[2]Department of Microbiology and Infectious Disease Center, School of Basic Medical Sciences, Peking University Health Science Center, 38 Xueyuan Road, Haidian District, Beijing 100191, P. R. China

[3]These authors contributed equally

[4]Lead contact

*Correspondence: yanghongying@suda.edu.cn

https://doi.org/10.1016/j.isci.2022.105115

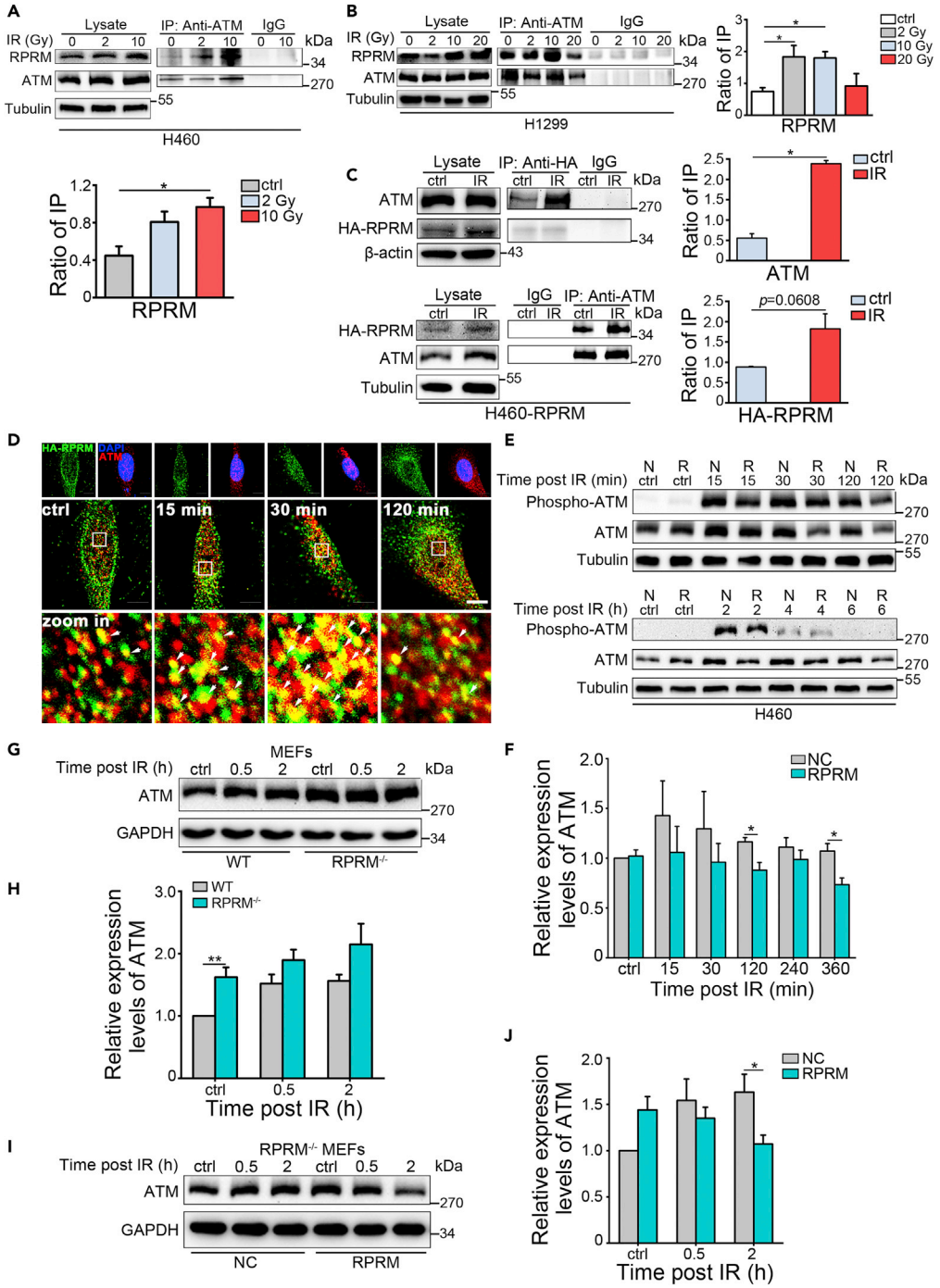

Figure 1. RPRM binds to ATM and down-regulates ATM levels

(A–C) Co-IP was performed 30 min after X-irradiation to demonstrate the interaction between ATM and RPRM in H460 (A), H1299 (B) and H460-RPRM (C) cells.

(D) Representative immunofluorescence images of co-localization of RPRM and ATM in RPRM$^{-/-}$ MEFs re-expressing RPRM at different times after 20 Gy X-irradiation.

(E and F) Change in the levels of total ATM and phospho-ATM in H460-NC (N)/RPRM (R) cells at different times after 2 Gy X-irradiation. Quantification of ATM levels (F), which was the average of three independent experiments.

(G and H) The ATM levels of WT MEFs were lower than those of RPRM$^{-/-}$ MEFs at different times after 20 Gy X-irradiation. Bar graph (H) shows quantification of ATM levels.

Figure 1. *Continued*
(I and J) RPRM re-expression reduced the ATM levels in RPRM$^{-/-}$ MEFs after 20 Gy X-irradiation. Bar graph (J) shows quantification of ATM levels.
Data shown represent the means (±SEM) of three biological replicates, *$p < 0.05$, **$p < 0.01$; significance was determined by unpaired two-sample t test.

cancers (Sato et al., 2006). Over-expressing RPRM not only results into G2/M cell-cycle arrest through inhibiting the activation of Cyclin B1·Cdc2 complex (Ohki et al., 2000), but also inhibits the cell proliferation, colony formation, migration and invasiveness of cancer cells (Buchegger et al., 2016, 2017; Ooki et al., 2013; Xu et al., 2012; Saavedra et al., 2015). Of interest, RPRM can be induced by X-irradiation and other genotoxic agents in a p53-dependent manner (Ohki et al., 2000; Ooki et al., 2013). Furthermore, RPRM overexpression enhances apoptosis induced by DNA damage agents (Ooki et al., 2013). These results suggest that RPRM may be involved in DDR pathway. However, whether and how RPRM is integrated in ATM signaling pathway remains unknown.

In this study, we identified RPRM as a novel negative regulator of ATM. Shortly after induction by X-irradiation, RPRM quickly translocated into the nucleus and interacted with ATM, promoted the nuclear export and degradation of ATM, leading to a reduction in ATM levels, impaired DNA repair and increased cellular sensitivity to DNA damage. We further revealed that RPRM phosphorylation at serine 98 mediated by cyclin-dependent kinase 4/6 (CDK4/6) was involved in the nuclear import of RPRM. Moreover, we found that Importin-11 (IPO11) was required for RPRM nuclear translocation, which was essential for its negative regulation on ATM. Furthermore, by using RPRM gene knockout (KO) mouse model, we confirmed the important role of RPRM in radiosensitivity *in vivo*. Thus, we discovered a novel crucial regulatory effect of RPRM on ATM and its consequences and we also revealed the underlying mechanism. These findings suggest that RPRM may be a novel potential target for both cancer therapy and radiation protection.

RESULTS

RPRM binds to ATM and down-regulates ATM levels

To determine the exact roles RPRM may play in DDR pathway, we first established a variety of cell lines with RPRM overexpression, namely H460-RPRM, A549-RPRM, AGS-RPRM, SNU-1-RPRM and HaCaT-RPRM (Figures S1A and S1B), as well as RPRM-deficient H460 and WS1 cells, pairing with their relevant negative control cells (NC) (Figures S1C and S1D). We also established a strain of RPRM KO mice using CRISPR-Cas9 technique, and obtained RPRM KO mouse embryonic fibroblasts (RPRM$^{-/-}$ MEFs). We confirmed an obvious RPRM induction after irradiation in RPRM wild-type (WT) MEFs (Figure S2A), which agreed with what was previously reported (Ohki et al., 2000). The rapid RPRM induction by IR was also observed in different human cancer cell lines and in cells with RPRM overexpression (Figures S2B and S2C).

Unexpectedly, by using co-immunoprecipitation (co-IP) assay, we found that endogenous RPRM interacted with ATM in both H460 and H1299 cells before and after exposed to IR (Figures 1A and 1B). The interaction was further confirmed in H460-RPRM cells, which was obviously enhanced after X-irradiation (Figures 1C and S3A). Using immunofluorescence microscopy, the co-localization of RPRM and ATM was observed in irradiated RPRM$^{-/-}$ MEFs re-expressing RPRM (Figures S1E and S1D) but not in irradiated RPRM$^{-/-}$ MEFs transfected with NC vectors (Figure S3B). These data indicate that RPRM binds to ATM, which is enhanced by irradiation.

More interestingly, we found that compared with H460-NC cells, H460-RPRM cells exhibited a reduction of up to 30% in the levels of total ATM protein after IR, which was especially significant at 2 h after X-irradiation and last for at least another 4 h, accompanied by a reduction in phosphorylated ATM (Figures 1E and 1F). Similar results were also observed in HaCaT human skin keratinocytes (Figure S4A), A549 lung cancer cells, AGS and SNU-1 gastric cancer cells (Figure S4B). These data suggest that RPRM down-regulates the levels of ATM protein after radiation exposure. To further confirm this, we also investigated how ATM levels would be changed by RPRM using RPRM$^{-/-}$ MEFs, and found that ATM levels were generally higher in RPRM$^{-/-}$ MEFs than in WT MEFs before and after irradiation (Figures 1G and 1H), implying that RPRM knockout increased ATM levels. However, this trend was reversed when RPRM was re-expressed in RPRM$^{-/-}$ MEFs and exposed to IR (Figures 1I and 1J). All these data indicate that irradiation-induced RPRM negatively regulates ATM protein levels.

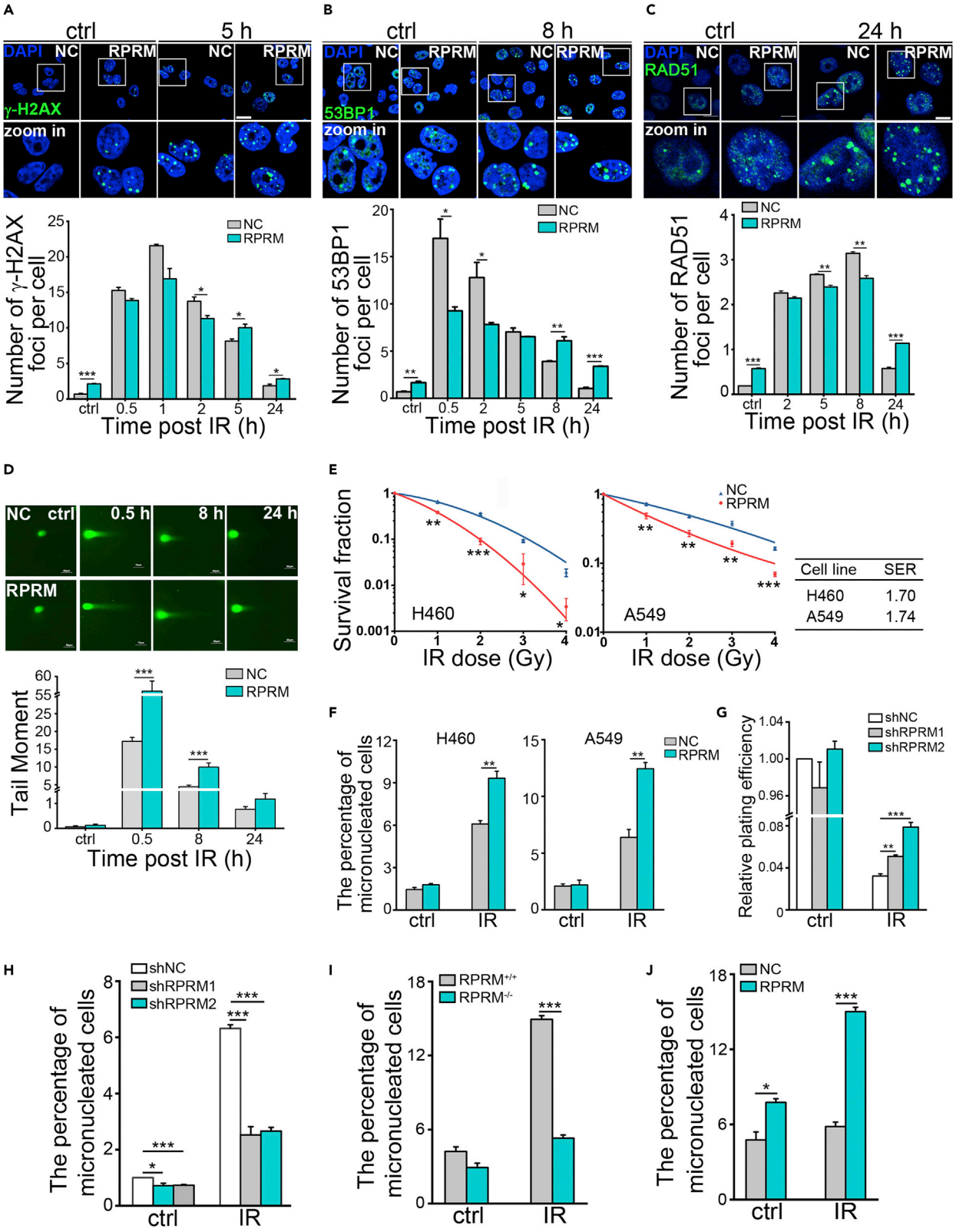
A
ctrl
5 h
DAPI NC RPRM NC RPRM
γ-H2AX
zoom in
Number of γ-H2AX foci per cell
NC
RPRM
Time post IR (h)
B
ctrl
8 h
53BP1
Number of 53BP1 foci per cell
C
ctrl
24 h
RAD51
Number of RAD51 foci per cell
D
NC ctrl
0.5 h
8 h
24 h
RPRM
Tail Moment
E
Survival fraction
H460
A549
IR dose (Gy)
Cell line SER
H460 1.70
A549 1.74
F
The percentage of micronucleated cells
G
shNC
shRPRM1
shRPRM2
Relative plating efficiency
H
I
RPRM+/+
RPRM-/-
J

Figure 2. RPRM inhibits DNA repair signaling pathway and enhances cellular radiosensitivity

(A) Representative immunofluorescence images of γ-H2AX in H460-NC/RPRM cells after 2 Gy X-irradiation and quantification of the number of γ-H2AX foci per cell. At least 200 nuclei were scored. Scale bars, 20 μm.

(B) Immunofluorescence images of 53BP1 foci after X-irradiated with 2 Gy and quantification. At least 200 nuclei were scored. Scale bar, 20 μm.

(C) Immunofluorescence images of RAD51 foci after IR and quantification. Scale bars, 10 μm. At least 500 nuclei for each sample were scored in each experiment.

(D) Comet assay on H460-NC/RPRM cells at different times after 2 Gy X-irradiation. The tail moments were quantified using CometScore. At least 500 cells were scored per sample. Scale bars, 50 μm.

(E) RPRM overexpression decreased the colony formation ability of cancer cells. Sensitization enhancement ratio (SER) was calculated according to the following formula: The radiation dose required for the control group to obtain 30% cell survival/the radiation dose required to obtain the same cell survival rate after overexpression of RPRM.

(F) RPRM overexpression increased micronucleus formation in cancer cells upon 2 Gy X-irradiation.

(G and H) RPRM knockdown significantly increased cellular radio-resistance manifesting as increased plating efficiency (G, 4 Gy) and decreased micronucleus formation (H, 2 Gy) in irradiated H460 cells.

(I) RPRM knockout significantly reduced the micronucleus formation in MEFs upon 5 Gy X-irradiation.

(J) Micronucleus formation of RPRM$^{-/-}$ MEFs transfected with NC and WT RPRM plasmids after exposed to 5 Gy X-irradiation.

Data shown represent the means (±SEM) of three biological replicates, *$p < 0.05$, **$p < 0.01$, ***$p < 0.001$; significance was determined by unpaired two-sample t test.

RPRM inhibits DNA repair signaling pathway and enhances cellular radiosensitivity

Owing to the vital role of ATM in DNA DSB repair, to investigate the consequences of the regulatory effect of RPRM on ATM, we then examined several important DSB repair indicators such as γ-H2AX foci, a widely used DNA DSB marker (Kinner et al., 2008), 53BP1, a critical protein for triggering non-homologous end joining (NHEJ) repair in DDR (Nakamura et al., 2006), and RAD51, a vital protein in catalyzing the core reactions of homologous recombination (HR) repair (Krejci et al., 2012). Both H2AX and 53BP1 are downstream substrates of ATM (Fernandez-Capetillo et al., 2002). RAD51 foci formed in the nuclei after radiation exposure represent repair foci through HR (Daboussi et al., 2002), in which ATM plays an important role (Takao et al., 1999). As shown in Figures 2A–2C, there was an elevated background of all three types of DNA repair foci in H460-RPRM cells compared with H460-NC cells, suggesting an elevated level of spontaneous DNA damage and repair caused by RPRM overexpression. However, at least within 2 h after irradiation H460-RPRM cells formed less γ-H2AX foci than H460-NC cells, but by 5 h after IR there were more γ-H2AX foci in H460-RPRM cells than in H460-NC cells, and this trend last up to 24 h after IR (Figures 2A and S5), suggesting that there existed more DSBs in irradiated cells with RPRM overexpression at longer time after IR. H460-RPRM cells formed less 53BP1 foci than H460-NC cells within 5 h after irradiation, although this trend was reversed by 8 h after irradiation, suggesting an NHEJ defect in H460-RPRM cells (Figures 2B and S6). Similarly, IR-induced RAD51 foci within 8 h after irradiation were less in H460-RPRM cells, but by 24 h after IR, H460-RPRM cells again exhibited considerably greater number of RAD51 foci than H460-NC cells (Figures 2C and S7), implying an HR defect in H460-RPRM cells. And the results indicating that these DSB repair-related proteins were all repressed in irradiated H460-RPRM cells were in agreement with the reduction in the total ATM levels and its activation (Figures 1E and 1F). To further confirm that RPRM did inhibit DNA DSB repair, we also examined the DNA DSB accumulation in cells at different times after IR by performing comet assay. As expected, compared with NC cells, the cells overexpressing RPRM showed greater DNA DSB accumulation after IR (Figure 2D), demonstrating that RPRM drastically attenuated DNA damage repair. All these data suggest that RPRM inhibits DNA damage repair signaling pathway probably via its down-regulatory effect on ATM.

Furthermore, overexpression of RPRM significantly increased the radiosensitivity of cancer cells manifesting as a reduction of colony-forming ability (Figures 2E, S8A, and S8B) and an increase in micronucleus formation (Figures 2F and S8C) upon irradiation when compared with NC cells. Conversely, RPRM knockdown significantly increased the plating efficiency of H460 cells (Figures 2G and S8D) and decreased the micronucleus formation of H460 (Figure 2H) and WS1 cells (Figure S8E) after IR, indicating that RPRM knockdown reduced cellular radiosensitivity. Moreover, although RPRM$^{-/-}$ MEFs formed much less micronuclei after radiation exposure than WT MEFs did (Figure 2I), re-expression of RPRM completely reversed the trend and significantly increased the micronucleus formation of RPRM$^{-/-}$ MEFs (Figure 2J). All these data indicate that RPRM plays a determining role in cellular radiosensitivity.

RPRM promotes ATM nuclear export and degradation

We further investigated how RPRM down-regulated ATM. We did not observe any significant reduction in ATM expression in irradiated cells with RPRM overexpression at mRNA level (Figure S9A), suggesting that

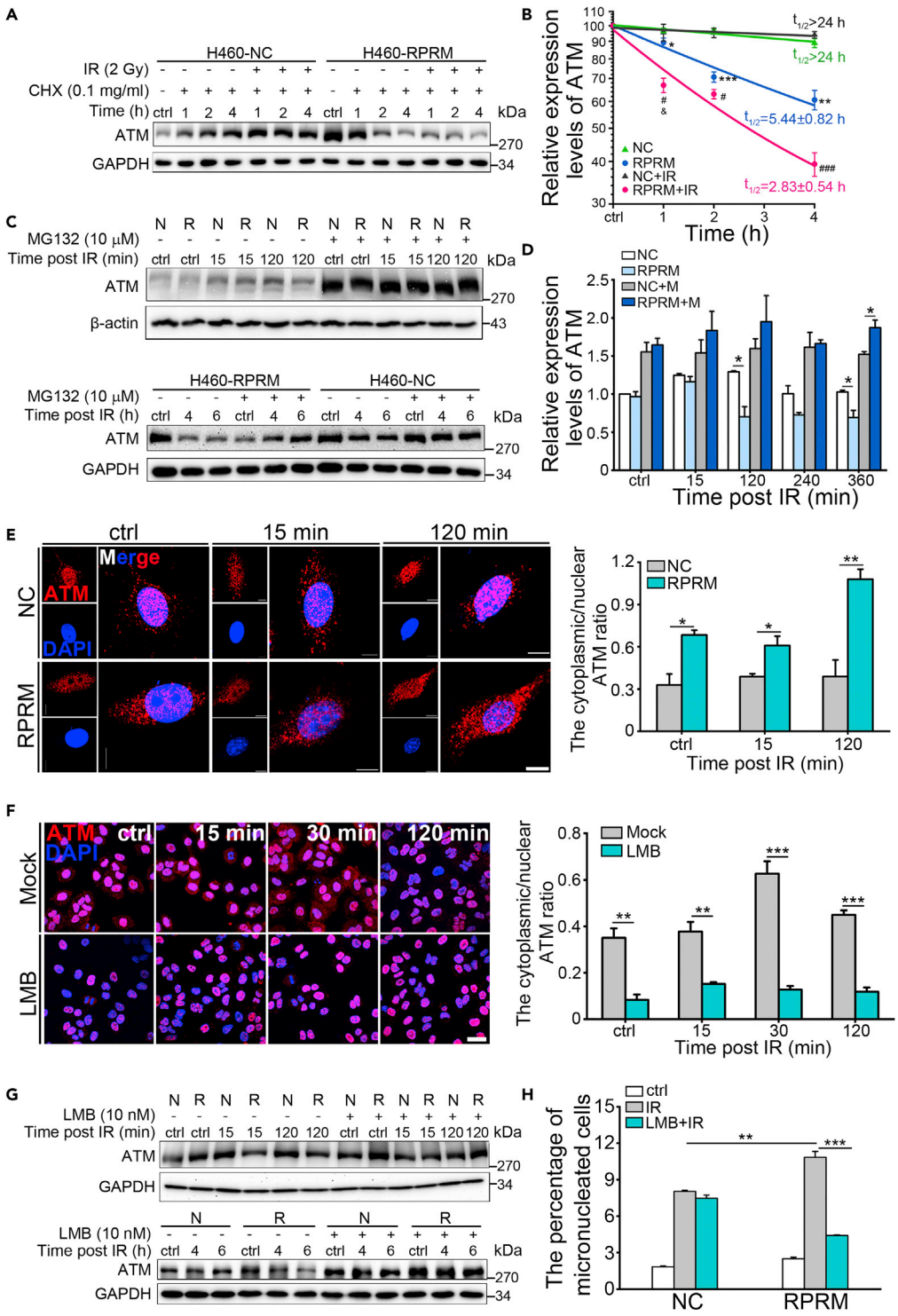

Figure 3. RPRM promotes the nuclear export and degradation of ATM

(A and B) Kinetics of the change in the ATM levels of H460-NC/RPRM cells with and without irradiation in the presence of cycloheximide (CHX, 0.1 mg/mL) examined by immunoblotting. (*, RPRM vs NC; #, RPRM + IR vs NC + IR; &, RPRM + IR vs RPRM).

(C and D) Change in the ATM levels of H460-NC (N)/RPRM (R) cells at the indicated time points after 2 Gy X-irradiation with and without MG132 (10 μM) pre-treatment.

Figure 3. *Continued*

(E) Change in the subcellular localization of ATM in RPRM$^{-/-}$ MEFs transfected with NC and RPRM vectors after 20 Gy X-irradiation and quantification of the ratios of cytoplasmic ATM fluorescence intensity to nuclear ATM fluorescence intensity. Scale bars, 10 μm.

(F) Representative immunofluorescence images of ATM in H460-RPRM cells pre-treated with leptomycin B (LMB, 10 nM) for 1 h at different times after 2 Gy X-irradiation and quantification of the cytoplasmic/nuclear ATM fluorescence intensity ratios. Scale bar, 20 μm.

(G) The effect of LMB pre-treatment on the total ATM levels of H460-NC/RPRM cells at different times after 2 Gy X-irradiation.

(H) Effect of LMB on the micronucleus formation of H460-NC/RPRM cells irradiated with 2 Gy X-rays.

Data shown represent the means (±SEM) of three biological replicates, *$p < 0.05$, **$p < 0.01$, ***$p < 0.001$, $^{\#}p < 0.05$, $^{\#\#\#}p < 0.001$, $^{\&}p < 0.05$; significance was determined by unpaired two-sample t test.

RPRM does not regulate ATM at transcription level. At protein level, in the presence of cycloheximide, a protein synthesis inhibitor, the ATM protein levels in H460-RPRM cells were significantly lower than those in H460-NC cells regardless of radiation exposure. The difference between H460-RPRM and H460-NC cells was much greater after irradiation (Figures 3A and 3B). The same result was observed in AGS-RPRM cells (Figure S9B). But this reduction of ATM levels in RPRM-overexpressed cells compared with NC cells was eliminated when treated with MG132, a proteasome inhibitor, prior to irradiation (Figures 3C and 3D). These data suggest that RPRM down-regulates ATM at protein level through promoting its degradation but not through inhibiting its synthesis. We further confirmed the effect of RPRM on ATM degradation using RPRM$^{-/-}$ MEFs. The ATM levels of RPRM$^{-/-}$ MEFs were slightly higher than those of WT MEFs with and without radiation exposure when the protein synthesis was inhibited, although the difference did not reach statistical significance (Figure S9C). However, re-expression of RPRM in RPRM$^{-/-}$ MEFs decreased the ATM levels, and the reduction was more significant after irradiation (Figure S9D), suggesting that RPRM promotes ATM degradation, resulting in a reduction of ATM levels, and this promotion is more obvious after irradiation.

Most proteins are degraded through ubiquitin-proteasome pathway, which may occur in both the cytoplasm and nucleus (Brooks et al., 2000). Although ATM is well known as a nuclear protein in dividing cells, missense mutations can lead to its abnormal cytoplasmic localization, which is correlated with its decreased expression (Jacquemin et al., 2012). Thus, we hypothesized that RPRM may enhance the nuclear export of ATM, in turn leading to its degradation and down-regulation. By using immunofluorescence microscopy, we found that compared with NC RPRM$^{-/-}$ MEFs, re-expression of RPRM significantly increased the cytoplasmic ATM levels and reduced the nuclear ATM levels before and after IR, leading to an increase in the ratio of cytoplasmic ATM to nuclear ATM (Figure 3E). We also observed an obvious increase in the cytoplasmic/nuclear ATM ratio when RPRM was overexpressed in H460 cells (Figures S10A and S10B), and the increase was much bigger after irradiation (Figures 3E, S10A, and S10B). Of interest, the phospho-ATM still predominantly accumulated in the nucleus (Figure S10C). The ATM translocation was also confirmed by immunoblotting on the cytoplasmic and nuclear fractions of cells, which clearly showed an increase in the cytoplasmic ATM levels and a reduction in the nuclear ATM levels in RPRM-overexpressing cells after IR (Figure S10D). Moreover, when leptomycin B (LMB), a widely used nuclear export inhibitor, was added into the culture of H460-RPRM cells, the cytoplasmic ATM levels were dramatically decreased whereas the nuclear ATM levels were increased, resulting in a significant reduction in the cytoplasmic/nuclear ATM ratios (Figure 3F). This suggested that the nuclear export of ATM induced by RPRM overexpression was diminished by LMB. At the same time, no reduction in the total ATM levels was detected (Figure 3G). Similar result was also obtained in RPRM$^{-/-}$ MEFs re-expressing RPRM (Figure S10E). These data indicate that RPRM enhances the nuclear export of ATM after IR, thus resulting in the reduction of the nuclear and total ATM levels. Additionally, LMB pre-treatment completely eliminated the increase of micronucleus formation in irradiated H460 cells caused by RPRM overexpression (Figure 3H), suggesting that the nuclear export of ATM was essential for the radiosensitizing effect of RPRM.

RPRM translocates from the cytoplasm to the nucleus upon irradiation, which involves CDK4/6

RPRM has been thought to be primarily localized in the cytoplasm since it was first reported (Ohki et al., 2000). Thus, our discovery that RPRM interacted with ATM and promoted its nuclear export implied that RPRM may translocate from the cytoplasm to the nucleus upon irradiation. We then explored whether IR changed the subcellular localization of RPRM. Of interest, H460-RPRM cells showed a significant increase

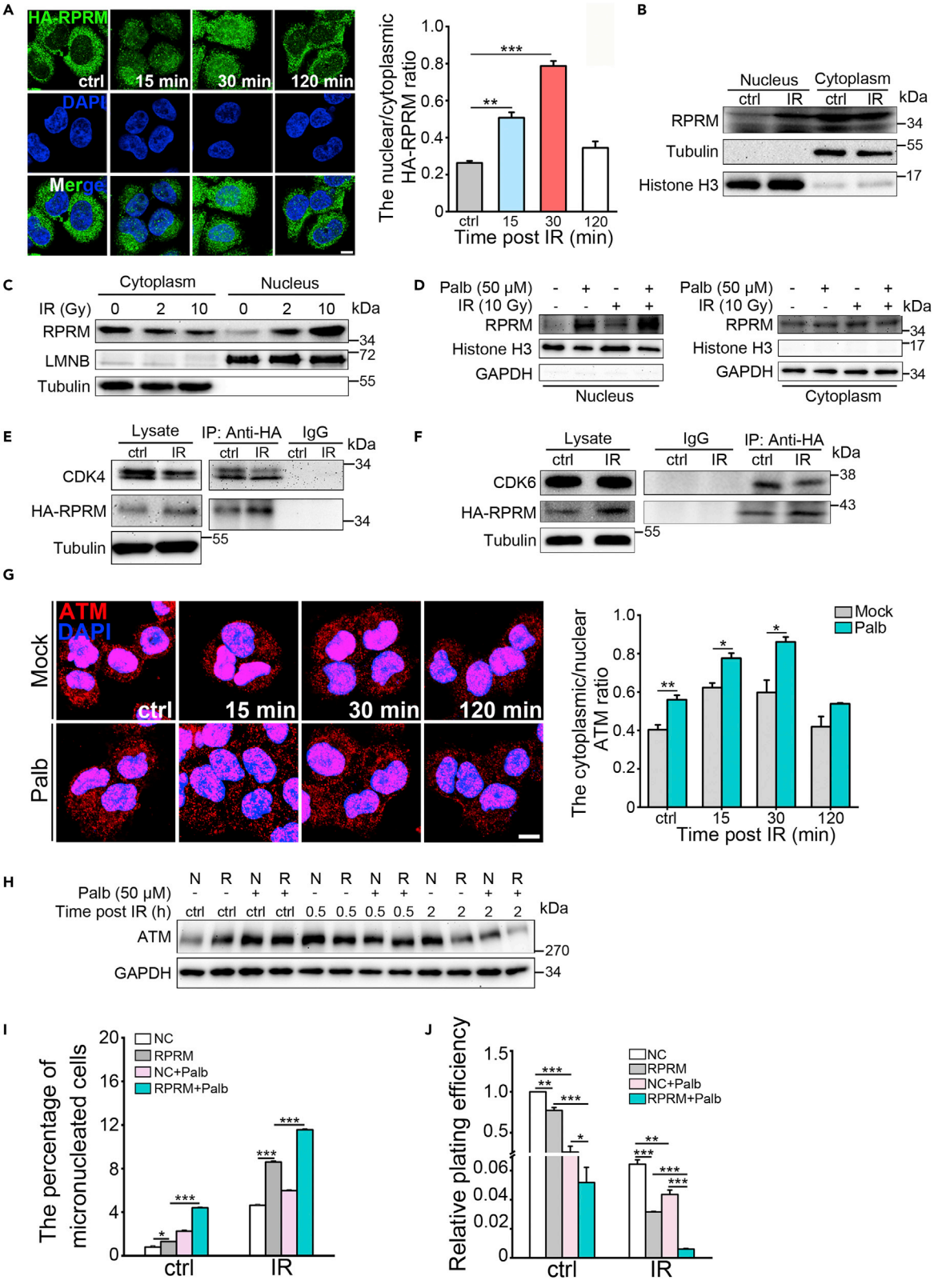
A
HA-RPRM
DAPI
Merge
ctrl
15 min
30 min
120 min
The nuclear/cytoplasmic HA-RPRM ratio
Time post IR (min)
B
Nucleus
Cytoplasm
RPRM
Tubulin
Histone H3
kDa
C
Cytoplasm
Nucleus
IR (Gy)
LMNB
D
Palb (50 μM)
IR (10 Gy)
GAPDH
E
Lysate
IP: Anti-HA
IgG
CDK4
F
CDK6
G
ATM
Mock
Palb
The cytoplasmic/nuclear ATM ratio
H
Time post IR (h)
I
The percentage of micronucleated cells
NC
RPRM
NC+Palb
RPRM+Palb
J
Relative plating efficiency

Figure 4. RPRM translocates from the cytoplasm to the nucleus upon irradiation, which involves CDK4/6

(A) Representative immunofluorescence images showing RPRM translocation from the cytoplasm to the nucleus in H460-RPRM cells shortly after 10 Gy X-irradiation and quantification of the nuclear/cytoplasmic HA-RPRM fluorescence intensity ratios. Scale bar, 10 μm.

(B) Immunoblotting on the nuclear and cytoplasmic RPRM of H460-RPRM cells 30 min after 10 Gy X-irradiation confirmed the nuclear translocation of RPRM upon IR.

(C) RPRM nuclear import was enhanced with the increase of irradiation dose.

(D) Immunoblotting on the nuclear and cytoplasmic RPRM confirmed that the nuclear translocation of RPRM was enhanced by palbociclib (Palb, 50 μM) pre-treatment.

(E and F) Co-IP result showing an interaction between RPRM and CDK4/6 in H460-RPRM cells.

(G) Inhibition of CDK4/6 promoted ATM nuclear export regulated by RPRM. Representative immunofluorescence images showing the effect of CDK4/6 inhibition by Palb pre-treatment on ATM cytoplasmic translocation in H460-RPRM cells upon 2 Gy X-irradiation and quantification of the ratios of cytoplasmic/nuclear ATM fluorescence intensity. Scale bar, 10 μm.

(H) Immunoblotting results confirmed that CDK4/6 inhibitor Palb reduced ATM levels in H460-NC/RPRM cells upon 2 Gy X-irradiation.

(I) The effect of CDK4/6 inhibition by Palb pre-treatment on the micronucleus formation of H460-NC/RPRM cells after 2 Gy X-irradiation.

(J) The effect of CDK4/6 inhibition by Palb pre-treatment on the plating efficiency of H460-NC/RPRM cells upon 4 Gy X-irradiation.

Data shown represent the means (±SEM) of three biological replicates, *$p < 0.05$, **$p < 0.01$, ***$p < 0.001$; significance was determined by unpaired two-sample t test.

in the immunofluorescence staining of RPRM in the nucleus 15 and 30 min after IR, but this increase was not observed by 2 h after IR (Figures 4A and S11A), indicating an occurrence of quick nuclear translocation of RPRM after its induction by IR. This nuclear translocation of RPRM was also confirmed by western blotting on the nuclear fractions of H460-RPRM cells (Figure 4B). Moreover, RPRM nuclear import was enhanced with the increase of irradiation dose (Figures 4C and S11B). These data demonstrate that RPRM translocates from the cytoplasm to the nucleus shortly after irradiation.

We further investigated how RPRM nuclear translocation was mediated. Of interest, pre-treating cells with palbociclib, a highly specific inhibitor of CDK4/6, prior to IR enhanced RPRM nuclear translocation, even palbociclib treatment alone could significantly increase the nuclear import of RPRM (Figures 4D and S11C), suggesting that CDK4/6 may play an important role in RPRM nuclear translocation. CDK4 has been found to interact with RPRM in a large-scale protein-protein interaction mapping by mass spectrometry (Ewing et al., 2007). Using co-IP assay, we confirmed that CDK4 indeed bound to RPRM in H460-RPRM cells and the interaction between CDK4 and RPRM was weakened after X-irradiation (Figure 4E). We found that CDK6 also interacted with RPRM and the CDK6-RPRM interaction was decreased after irradiation (Figure 4F). This may be associated with the decreased levels of CDK4/6 in irradiated H460-RPRM cells (Figures S11D and S11E), which coincided with the nuclear translocation of RPRM (Figure 4A). Furthermore, with palbociclib, the cytoplasmic ATM levels of cells were significantly increased before and after IR whereas the nuclear ATM levels were obviously decreased, leading to a significant increase in the cytoplasmic/nuclear ATM ratios (Figure 4G). Moreover, the total ATM levels were markedly reduced by palbociclib in both H460-RPRM and H460-NC cells after exposed to X-rays (Figure 4H). This indicated that CDK4/6 inhibition promoted ATM nuclear export and decreased ATM protein levels. Furthermore, the radiosensitivity of H460-NC and H460-RPRM cells was enhanced when pre-treated with palbociclib, and this increase was more significant in H460-RPRM cells (Figures 4I and 4J). Taken together, these data suggest that CDK4/6 are involved in the nuclear translocation of RPRM and its negatively regulatory effect on ATM and cellular radiosensitivity.

CDK4/6 phosphorylates RPRM at serine 98, the unphosphorylation status of RPRM is critical for its stabilization and nuclear translocation

Because RPRM contains a predicated phosphorylation site at serine 98 (Amigo et al., 2018), and CDK4/6 are members of Ser/Thr protein kinase family, we then performed mass spectrometry analysis to determine whether CDK4/6 could directly phosphorylate RPRM. Not unexpectedly, CDK4/6 indeed phosphorylated RPRM at serine 98 (Figures 5A and 5B), indicating that CDK4/6 regulates RPRM via a post-translational mechanism. Moreover, after CDK4/6 inhibition by palbociclib, the RPRM levels of H460-RPRM cells were obviously increased, which was similar to its change in the presence of MG132 (Figure 5C), suggesting that unphosphorylated RPRM may have greater stability. To further explore whether the phosphorylation of RPRM at serine 98 mediated by CDK4/6 was critical to its nuclear translocation and its negatively regulatory effect on ATM as well as cellular radiosensitivity, we generated RPRM point mutant (S98A) and deletion mutant (Δ(79–109)) constructs without the phosphorylation site (Figure 5D), and transiently expressed HA-tagged full-length RPRM and RPRM mutant constructs in RPRM$^{-/-}$ MEFs. Both mutants translocated

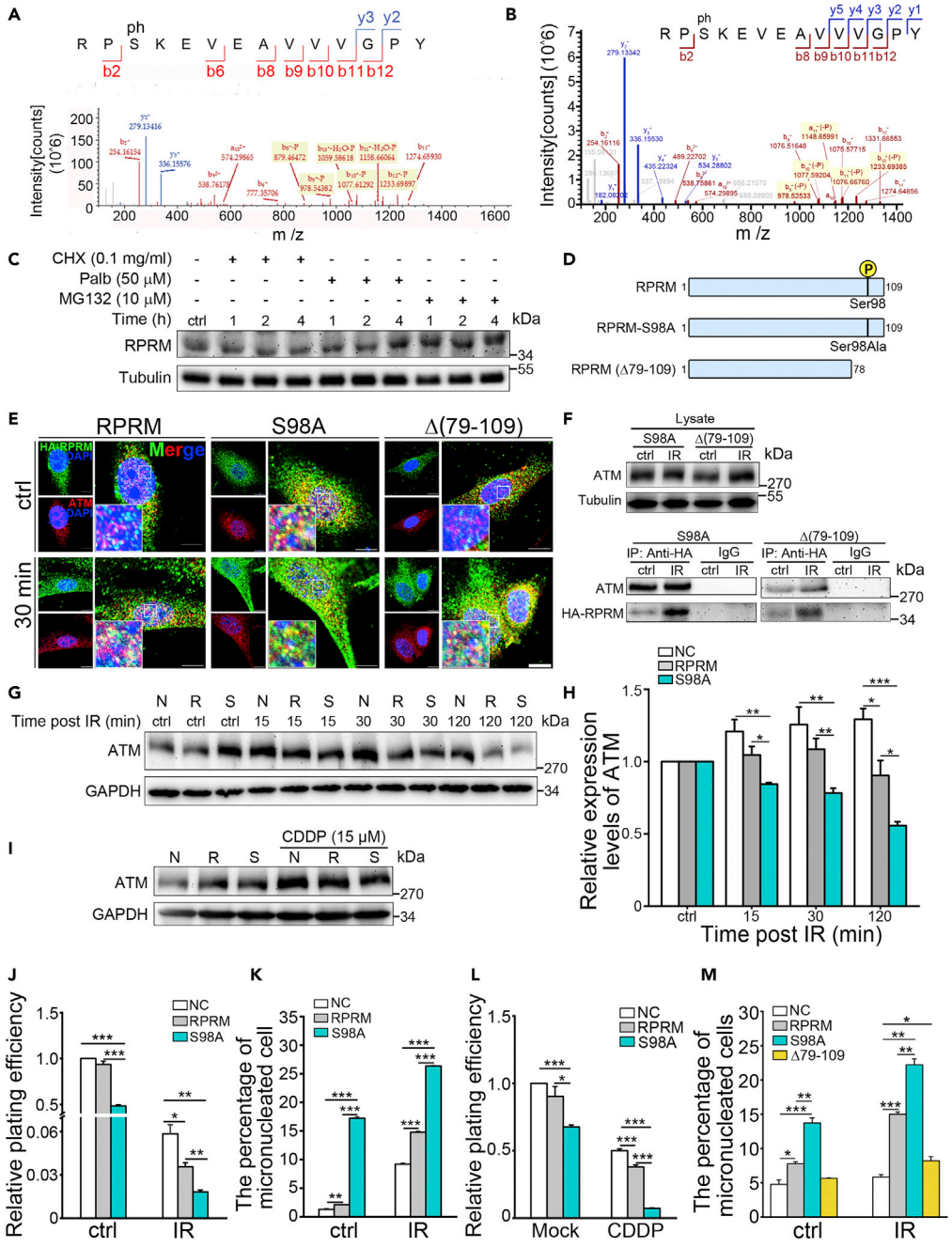

Figure 5. CDK4/6 phosphorylate RPRM at serine 98, but the unphosphorylation status of RPRM is critical for its stabilization and nuclear translocation

(A and B) Mass spectrometry analysis of the phosphorylation site of RPRM corresponding to CDK4 (A) and CDK6 (B).

(C) Time-course analysis of the changes in the RPRM levels of H460-RPRM cells after treated with different inhibitors.

(D) Diagrams of full-length RPRM protein and different mutants.

(E) Representative immunofluorescence images of the RPRM$^{-/-}$ MEFs exogenously expressing full-length RPRM, RPRM-S98A and ΔRPRM (79–109) at 30 min after 20 Gy X-irradiation. Scale bars, 10 μm.

(F) Co-IP assay confirmed an interaction between ATM and both RPRM-S98A and ΔRPRM (79–109) in H460 cells.

(G and H) Change in the ATM levels of H460-NC/RPRM/S98A cells at different times after 2 Gy X-irradiation.

(I) Change in the ATM expression of H460-NC/RPRM/S998A cells after cisplatin (CDDP, 15 μM) treatment for 24 h.

(J) Relative plating efficiency of H460-NC/RPRM/S98A cells irradiated with 4 Gy X-rays.

Figure 5. *Continued*

(K) Exogenous expression of both RPRM and RPRM-S98A increased micronucleus formation in H460 cells upon 2 Gy X-rays.

(L) Relative plating efficiency of H460-NC/RPRM/S98A cells treated with 15 μM CDDP.

(M) Micronucleus formation of RPRM$^{-/-}$ MEFs expressing full-length RPRM, RPRM-S98A and ΔRPRM (79–109) after exposed to 5 Gy X-irradiation.

Data shown represent the means (±SEM) of three biological replicates, *p < 0.05, **p < 0.01, ***p < 0.001; Significance was determined by unpaired two-sample t test.

from the cytoplasm to the nucleus shortly after IR just like full-length RPRM did (Figure 5E). However, the truncated mutant exhibited much less nuclear accumulation compared with RPRM-S98A mutant, implying that the intricate mechanism of RPRM translocation may involve its phosphorylation status and its structural integrity of C-terminal domain. Of interest, both point and deletion mutants interacted with ATM (Figures 5E and 5F), suggesting that its C-terminal residues (79–109) may not be essential for the interaction between ATM and RPRM. In agreement with the robust nuclear translocation of the RPRM-S98A mutant and its interaction with ATM, the ATM protein levels of H460-S98A cells was much lower than those of H460-NC/RPRM cells under DNA damage stress such as IR and cisplatin treatment (Figures 5G–5I). It was worth noting that the basal level of RPRM protein in H460-S98A cells was higher than that of H460-NC/RPRM cells (Figure S12), which is consistent with the result that unphosphorylated RPRM was more stable. However, no obvious difference in the RPRM induction was observed in H460-NC/RPRM/S98A cells after IR and cisplatin treatment (Figure S12). All these data suggest that CDK4/6 phosphorylate RPRM at serine 98, but preventing RPRM phosphorylation makes it more stable and more easily to translocate to the nucleus, thus resulting in a greater reduction in ATM levels, moreover, the negative regulation of RPRM on ATM depends more on its nuclear import than on its induction.

Because the phosphorylation status of RPRM was crucial to the nuclear translocation of RPRM and its regulation on ATM, we also explored how RPRM phosphorylation affected cellular sensitivity to DNA damage. As shown in Figures 5J–5L, exogenously expressing PRRM-S98A mutant alone caused a greater reduction in colony formation and a greater increase in the background micronucleus frequency in H460 cells than overexpressing full-length RPRM did. Moreover, H460 cells with PRRM-S98A mutant expression showed much greater sensitivity to DNA damaging agents such as IR and cisplatin. To further confirm the result that inhibition of RPRM phosphorylation confers cellular sensitivity to DNA damage, using RPRM$^{-/-}$ MEFs expressing full-length RPRM, RPRM-S98A and ΔRPRM (79–109) mutants, we found that compared with the negative control RPRM$^{-/-}$ MEFs and RPRM$^{-/-}$ MEFs re-expressing full-length RPRM, the RPRM$^{-/-}$ MEFs expressing PRRM-S98A mutant exhibited higher background and radiation-induced micronucleus frequency, suggesting that inhibition of RPRM phosphorylation enhanced the sensitivity of normal cells to spontaneous and IR-induced DNA damage (Figure 5M). It was also worth noting that expressing ΔRPRM (79–109) mutants only caused a slight but significant increase in micronucleus formation after IR when compared with NC (Figure 5M), suggesting that an intact C-terminal domain of RPRM was also important to its radiosensitizing effect in addition to its unphosphorylation status. These data indicate that for both cancer and normal cells, inhibition of RPRM phosphorylation confers cellular sensitivity to DNA damage. This supports our observation that the negatively regulatory effect of RPRM on ATM involves RPRM phosphorylation mediated by CDK4/6 and ATM nuclear export.

IPO11 is essential for the nuclear translocation of RPRM upon irradiation

Given that the active transport of proteins between the cytoplasm and the nucleus is mediated by karyopherin/importin transport receptors (Görlich and Kutay, 1999; Chook and Blobel, 2001), and IPO11, a member of importin-beta family, can interact with RPRM (Huttlin et al., 2021), we then hypothesized that IPO11 may play an important role in RPRM nuclear import. First, using co-IP, we demonstrated that RPRM did bind to IPO11, and the interaction was enhanced in H460-RPRM cells upon irradiation (Figure 6A). The RPRM-IPO11 interaction was also confirmed by their co-localization in RPRM$^{-/-}$ MEFs re-expressing RPRM (Figure 6B) and H460-RPRM cells (Figure S13A) using immunofluorescent microscopy. Moreover, consistent with the increase of the nuclear translocation of un-phosphorylated RPRM (Figure 5E), RPRM S98A mutant showed stronger interaction with IPO11 than WT RPRM did before and after IR (Figure S13B).

To test the role of IPO11 in RPRM nuclear translocation, we knocked out IPO11 in H460-RPRM cells using CRISPR-Cas9 technique. Not unexpectedly, we found that IPO11 knockout strongly blocked RPRM nuclear import after IR as detected by immunofluorescence microscopy (Figure 6C) and western blotting on the nuclear

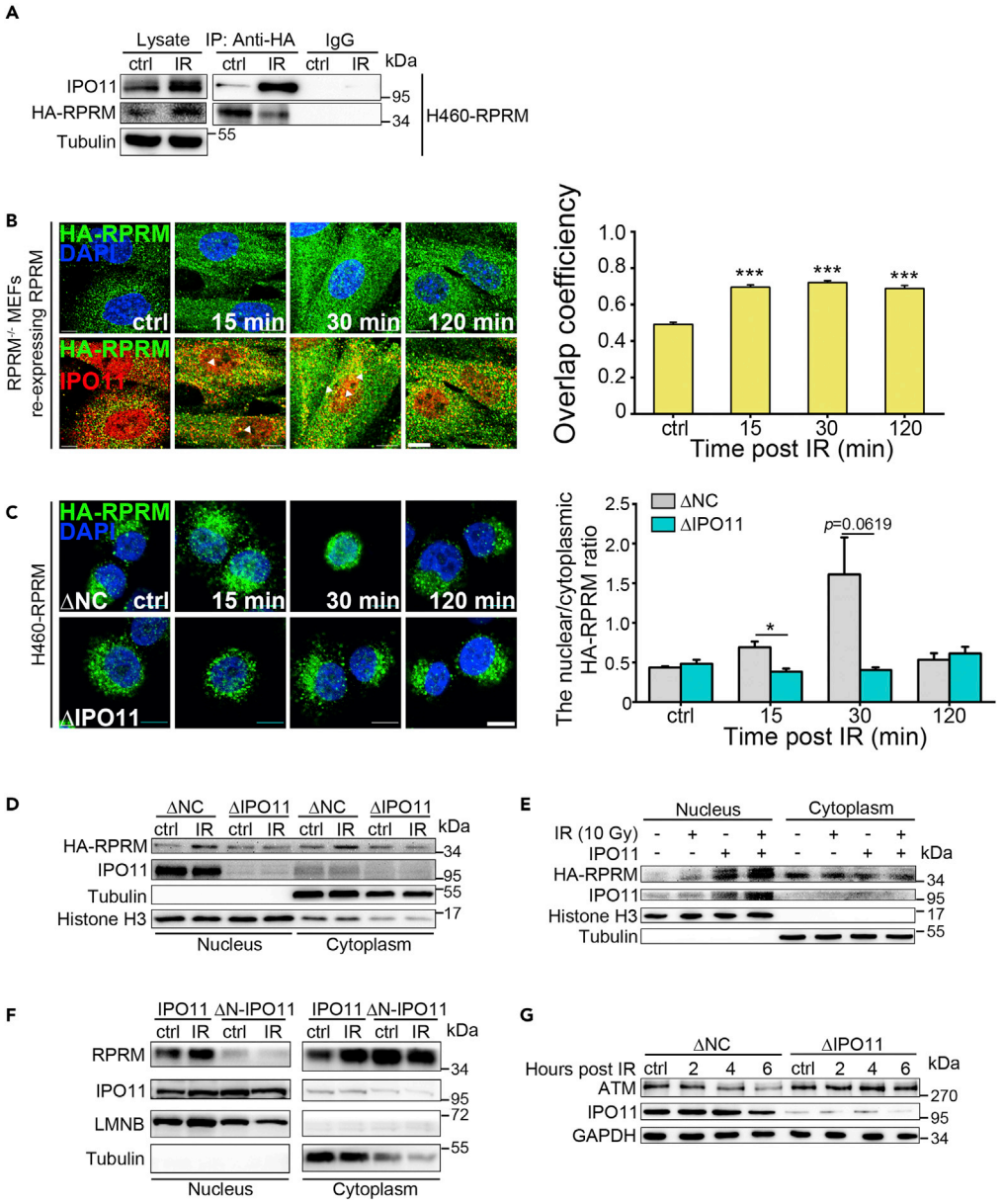

Figure 6. IPO11 is essential for the nuclear translocation of RPRM upon irradiation

(A) An interaction between RPRM and IPO11 in H460-RPRM cells was confirmed by Co-IP performed 30 min after 10 Gy X-irradiation.

(B) Representative immunofluorescence images of co-localization of RPRM (green) and IPO11 (red) in RPRM$^{-/-}$ MEFs re-expressing RPRM. Scale bar, 10 μm.

(C) Change in the subcellular localization of RPRM in negative control H460-RPRM cells (ΔNC) and cells with IPO11 deletion (ΔIPO11) after 10 Gy X-irradiation. Scale bars, 10 μm.

(D) Immunoblotting on the nuclear and cytoplasmic RPRM of H460-RPRM-ΔNC/ΔIPO11 cells 30 min after 10 Gy X-irradiation.

(E and F) Changes in the nuclear and cytoplasmic RPRM in IPO11-deleted H460-RPRM cells re-expressing WT IPO11 (E) and dominant-negative IPO11 mutant (F) 30 min after 10 Gy X-irradiation.

(G) Change of ATM protein levels in H460-RPRM-ΔNC/ΔIPO11 cells after 2 Gy X-irradiation.

Data shown represent the means (±SEM) of three biological replicates, *p < 0.05, ***p < 0.001; significance was determined by unpaired two-sample t test.

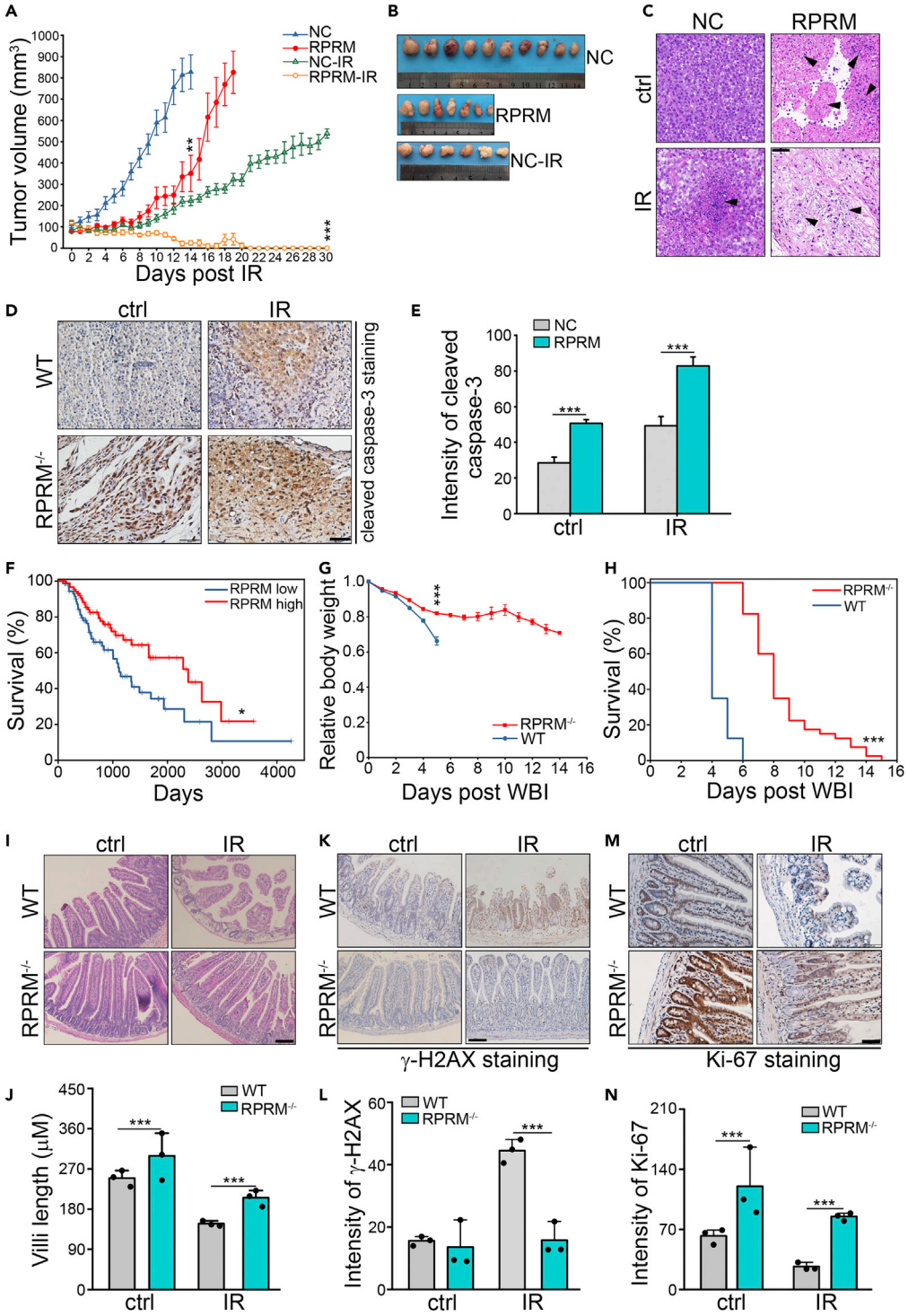

Figure 7. RPRM is a potential target for cancer therapy and radiation protection

(A and B) Comparison of the tumor growth of the four groups after a single dose of 5 Gy of X-irradiation. Tumor volumes (A) calculated by the formula: volume=(length)×(width)^2/2 (mice: n = 10 for NC, n = 7 for RPRM, n = 6 for NC + IR, n = 5 for RPRM + IR) and representative pictures of tumors (B) excised on day 14 (NC), 18 (RPRM), 30 (NC-IR) after IR, respectively. Pictures of irradiated tumors with RPRM overexpression were not provided because the tumors shrank completely by the end of observation.

Figure 7. *Continued*

(C) H&E staining of the tumor sections showing that RPRM overexpression caused more severe cell death. Scale bar, 50 μm. Black arrows indicate apoptosis of tumor cells.

(D and E) Immunohistochemistry staining of cleaved caspase-3 of the tumor sections. Positive cells were counted by using Image J (n = 3 for each group). Scale bar, 50 μm.

(F) The cancer genome atlas (TCGA) lung squamous cell carcinoma dataset shows that the clinical outcome after radiotherapy (10-year overall survival) was associated with the expression of RPRM. Kaplan-Meier survival curves and Log-rank statistics are shown.

(G) Changes of normalized body weights of RPRM$^{-/-}$ and WT mice after receiving 9 Gy WBI showed a more dramatic decline in the body weights of WT mice than in those of RPRM$^{-/-}$ mice.

(H) Kaplan-Meier analysis of the survival of WT and RPRM knockout mice after receiving 9 Gy WBI (n = 40 for each group including 20 male and 20 female mice).

(I and J) H&E staining of the small intestines of RPRM$^{-/-}$ and WT mice on day 3.5 after 9 Gy WAI. Villi length was quantified using cellSens Standard 1.8.1 (n = 3 for each group). Scale bar, 100 μm.

(K and L) Immunohistochemistry staining of γ-H2AX on day 3.5 after 9 Gy WAI. Positive cells were counted by using image-pro plus 6.0 (n = 3 for each group). Scale bar, 100 μm.

(M and N) Immunohistochemistry staining of Ki-67 on day 3.5 after 9 Gy WAI. Positive cells were counted by using image-pro plus 6.0 (n =3 for each group). Scale bar, 50 μm.

Data shown represent the means (±SEM) of at least three biological replicates, *$p < 0.05$, **$p < 0.01$, ***$p < 0.001$; significance was determined by two-way ANOVA with Tukey's correction (A and G) or unpaired two-sample t test (E, J, L, and N). Survival of mice and cancer patients was presented using Kaplan-Meier curves and significance was assessed using logrank test (F and H).

fractions (Figure 6D). These data suggested that IPO11 was required for RPRM nuclear import. To further determine the essential role of IPO11 in RPRM transport, we re-expressed WT IPO11 and dominant-negative IPO11 mutant (ΔN-IPO11, Figure S13C) in IPO11-deleted H460-RPRM cells. As shown in Figures 6E and 6F, IR-induced RPRM nuclear import was restored in cells re-expressing WT IPO11, but not in cells expressing mutant IPO11. Collectively, these data indicate that IPO11 is essential for RPRM nuclear import upon irradiation. Accordingly, IPO11 deletion eliminated the reduction in the ATM protein levels of H460-RPRM cells after irradiation (Figure 6G), confirming the critical role of IPO-11mediated RPRM nuclear import in its negative regulation on ATM.

Besides, it was worth noting that there existed a small amount of nuclear RPRM prior to irradiation even when IPO11 was deleted, which did not increase after IR (Figures 6C and 6D). This suggests that in addition to its major cytoplasmic localization, RPRM also localizes in the nucleus in small quantities, which is independent of IPO11.

RPRM is a potential target for cancer therapy and radiation protection

To further confirm the determining role of RPRM in radiosensitivity, we performed xenograft assay, and found that RPRM overexpression not only significantly inhibited tumor growth, which agreed with its tumor suppressor characteristics (Amigo et al., 2018; Buchegger et al., 2017; Ooki et al., 2013; Xu et al., 2012), but also sensitized tumors to radiotherapy (Figures 7A and 7B). With hematoxylin and eosin (H&E) and immunohistochemistry staining, we observed that the tumors formed by H460-RPRM cells grew in loose clusters and showed a feature of high differentiation, pleomorphism, extensive keratinization and spontaneous apoptosis (Figures 7C–7E). In contrast, the tumors formed by H460-NC cells exhibited a feature of strong basophilia, low differentiation and keratinization (Figure 7C). Moreover, IR exposure enhanced apoptosis more substantially in H460-RPRM cell-formed tumors than in H460-NC cell-formed tumors (Figures 7C–7E).

To further determine the therapeutic relevance of RPRM in cancers, we performed TCGA analysis. According to the TCGA lung squamous cell cancer database, good prognosis of lung cancer patients after radiotherapy was associated with high RPRM mRNA expression (Figure 7F). The same tendency was observed in glioma patients (Figure S14). All these data indicate that RPRM is a potential therapeutic target for certain types of cancer.

Furthermore, we investigated the radiosensitivity of RPRM knockout mice. RPRM knockout mice appeared normal and were indistinguishable from their WT littermates (Figures S15A and S15B). After whole body irradiation (WBI), compared with WT mice that lost weight sharply and all died within 6 days, RPRM knockout mice lost less weight and even made a slight improvement 7 days after WBI before the second wave of weight loss starting on day 11, and eventually all died within 15 days after WBI (Figures 7G and 7H). Both male and female RPRM knockout mice showed similar results (Figures S15C and S15D), although

it seemed that RPRM knockout had better protective effect on male mice than on female mice (Figure S15E). These data indicated that RPRM knockout significantly delayed mouse death after exposed to WBI. Moreover, we examined radiation-induced intestinal injury in RPRM knockout mice. After whole abdominal irradiation (WAI), compared with WT mice, RPRM knockout mice showed much less severe villus injury (Figures 7I and 7J), less DNA damage (γ-H2AX) (Figures 7K and 7L) and more cell proliferation (Ki67) in small intestine (Figures 7M and 7N), indicating that RPRM knockout dramatically protected mice against radiation-induced intestinal injury. All these results indicate that RPRM deficiency protects mice from IR-induced damage, thus RPRM may serve as a target for radiation protection. Taken together, it is confirmed *in vivo* that RPRM is a potential target for cancer treatment and radiation protection.

DISCUSSION

Here, we discovered that RPRM, a poorly understood protein, is actually an important novel regulator of ATM. Specifically, RPRM down-regulates ATM protein levels and inhibits DNA damage repair, thus enhancing cellular sensitivity to genotoxic agents. After induced by DSBs, RPRM rapidly translocates from the cytoplasm to the nucleus, interacts with ATM and promotes its nuclear export and proteasomal degradation resulting in a reduction of ATM levels. Furthermore, we revealed that the nuclear translocation of RPRM not only involves its phosphorylation at serine 98 mediated by CDK4/6, but also requires IPO11.

Despite the intensive investigation into the vital role of ATM as an apical conductor of DDR relaying a widespread signal to a variety of downstream effectors in response to DNA DSBs (Marechal and Zou, 2013; Shiloh, 2003; Kastan and Lim, 2000; Shiloh and Ziv, 2013; Matsuoka et al., 2007), the molecular mechanisms underlying how ATM itself is regulated, in particular shortly after DNA damage induction, remain to be elucidated. In this study, we found that ATM expression levels declined conspicuously in RPRM-overexpressed cells soon after the induction of DNA DSBs. Moreover, RPRM modulated the down-regulation of ATM at protein level but not at mRNA level. More specifically, RPRM down-regulated ATM protein by promoting its nuclear export and proteasomal degradation. And inhibiting ATM nuclear export by leptomycin B reversed the down-regulation of ATM by RPRM. This suggested that the degradation and down-regulation of ATM were associated with its cytoplasmic localization. This agrees with what was previously reported that the total ATM protein level is positively correlated with its nuclear localization and ATM under-expression is linked to its abnormal cytoplasmic localization (Jacquemin et al., 2012). Of interest, although it was previously reported that exposure to IR or etoposide induces the nuclear-cytoplasmic translocation of activated ATM (Hinz et al., 2010), we did not observe any increase in the phosphorylated ATM levels in the cytosol of the irradiated cells overexpressing RPRM, indicating that RPRM promoted only the nuclear-cytoplasmic translocation of ATM but not that of activated ATM. This may result in different consequences, whereas the nuclear export of activated ATM triggers NF-κB activation (Hinz et al., 2010), the nuclear export of ATM leads to its degradation and down-regulation. Thus, our results provide a potential mechanism for ATM down-regulation, i.e., degradation because of its abnormal cytoplasmic localization mediated by RPRM, although further studies are required to clarify the detailed mechanisms underlying how ATM is transported from the nucleus to the cytoplasm and how it is degraded there. In addition to the canonical function of ATM in DNA damage repair signaling pathway, which is dependent on its nuclear localization, accumulating evidence shows that cytoplasmic ATM may play some roles in Akt activation, autophagy in response to oxidative stress, etc (Tapodi et al., 2019; Alexander et al., 2010). Therefore, our finding that RPRM-overexpressed cells containing higher cytoplasmic ATM levels may suggest that their ATM may function differently from that in the parental cells. It will be worth investigating what functions the cytoplasmic ATM may have when RPRM is overexpressed.

Overexpression of RPRM has been reported to induce G2/M arrest (Ohki et al., 2000). However, here we found that overexpression of RPRM alone did not obviously affect the cell cycle distribution in H460 cells, neither did it cause G2/M arrest compared with the NC group 2 h after 2 Gy X-irradiation (unpublished data), at which a significant reduction in ATM level was observed. Furthermore, the ATM protein level was not decreased when H460-NC cells were treated with nocodazole (ND), a widely-used cell cycle synchronizing agent, to be arrested at G2/M phase (unpublished data). These results suggest that the negative regulation of RPRM on ATM is not associated with G2/M arrest. However, since we also found an involvement of CDK4/6, which play an important role in cell cycle regulation through phosphorylating the downstream cell cycle-related proteins such as Rb (Harbour et al., 1999), in the nuclear translocation of RPRM and its regulatory effect on ATM, it will be worth investigating further how cell cycle affects the novel role of RPRM in DDR in the future.

RPRM has been proposed as a cytoplasmic protein since it was identified (Ohki et al., 2000). However, in the present study, we discovered that RPRM also localizes in the nucleus despite its small amount. Most importantly, RPRM can translocate rapidly from the cytosol to the nucleus under DNA damage stress. We further found that the nuclear transport of RPRM was governed by CDK4/6-mediated phosphorylation of RPRM at serine 98. Inhibition of CDK4/6 by palbociclib or serine 98 point mutation of RPRM protein promoted the nuclear translocation of RPRM, which was very likely because of its unphosphorylation and stabilization. This is in accordance with previous reports that site-specific phosphorylation of proteins such as p53 and neurofibromatosis-2 leads to their degradation by ubiquitination (Bech-Otschir et al., 2001; Tang et al., 2007). Furthermore, we confirmed an interaction between RPRM and IPO11. As a nuclear transport receptor, IPO11 facilitates the transport of its cargo proteins such as class-III E2 enzymes, PTEN, BZW1 and BZW2 from the cytoplasm to the nucleus through nuclear pore complexes (Zhang and Matunis, 2005; Chen et al., 2017; Nachmias et al., 2022). We further demonstrated that IPO11 is required for RPRM nuclear import, thus suggesting that RPRM is a novel cargo protein of IPO11.

We revealed that the nuclear import of RPRM mediated by CDK4/6 and IPO11 is an important mechanism for regulating its subcellular localization and function. The function of a protein is usually associated with its subcellular localization. Our finding on the change in the subcellular localization of RPRM upon DNA damage indicates that RPRM has some novel functions related to its nuclear translocation, e.g. its negatively regulatory effects on ATM and DNA repair. As a result of the un-phosphorylation of RPRM and its nuclear translocation mediated by CDK4/6 inhibition, more ATM was exported from the nucleus and degraded, resulting in lower ATM levels, impaired DNA repair and greater cellular sensitivity to DNA damage. There is some evidence suggesting that ATM may be associated with CDK4. When activated through CDK4-mediated phosphorylation, the E3 ligase WSB1 promotes ATM ubiquitination and degradation (Kim et al., 2017). Our results establish a novel connection between CDK4/6 and ATM, which is that CDK4/6 indirectly modulates ATM levels and activation through RPRM. Interestingly, compare with the interaction between RPRM and CDK4, the interaction between RPRM and CDK6 was not decreased that obviously, although it was still slightly lower than that before IR. This suggests that CDK6 may not as important as CDK4 in the regulation of RPRM nuclear translocation after IR even though it can phosphorylate RPRM. We also provide another potential mechanism for the inhibition of ATM activation by CDK4/6 inhibitor palbociclib leading to weakened DNA repair and increased radiosensitivity other than through protein phosphatase 5 (Huang et al., 2018). Furthermore, we demonstrated that IPO11 deletion up-regulates ATM levels in RPRM-overexpressing cells. This not only indicates the necessity of RPRM nuclear import for its regulation on ATM, but also reveals a critical role of IPO11 in the function of RPRM through transporting it from the cytoplasm to the nucleus.

The previous studies have suggested that RPRM may be involved in cell-cycle arrest and apoptosis induced by DNA damage (Ohki et al., 2000; Ooki et al., 2013). But whether it participates DNA repair pathway remain unknown. In this study, in agreement with its nuclear translocation upon DNA damage as we described above, we clearly demonstrated that RPRM plays an important novel role in DNA DSB repair. We found that RPRM overexpression inhibited both HR and NHEJ pathways resulting in impaired DNA damage repair and more DSB accumulation, in turn increased cellular radiosensitivity. This may be associated with its negatively regulatory effect on ATM. These results were consistent with the hypersensitivity of ATM-mutated cancer cells and A-T cells to IR (Ahmed et al., 2016; Chun and Gatti, 2004). Inhibiting DDR pathway is one of the important mechanisms underlying the capability of sensitizers to sensitize cancer cells to genotoxic agents (Goldstein and Kastan, 2015). Thus, proteins that play critical roles in DDR such as ATM, CDK4/6, etc. have been proposed as important therapeutic targets for cancer therapy. Several ATM inhibitors and CDK4/6 inhibitors have been demonstrated to exhibit a synergistic effect with radiotherapy both *in vitro* and *in vivo* (Zhang et al., 2015; Karlin et al., 2018; Riches et al., 2019; Huang et al., 2018; Göttgens et al., 2019; Pesch et al., 2020). Early clinical development has also been initiated to explore the implication of some ATM inhibitors (Jin and Oh, 2019). Here we identified RPRM as a critical protein in DNA damage repair pathways. We also confirmed its inhibitory effect on tumor growth, which is in agreement with its tumor suppressor properties (Amigo et al., 2018; Buchegger et al., 2017). These results indicate that RPRM may serve as a novel target for cancer therapy. Furthermore, it is worth pointing out that RPRM may inhibit DNA repair through targets other than ATM. Since the phosphorylation of 53BP1 and the focus formation may involve ATM, ATR, and DNA-PKcs (Anderson et al., 2001), our results showing inhibited 53BP1 foci formation when RPRM was overexpressed did not

rule out the possibility of the regulatory effect of RPRM on ATR and DNA-PKcs. As a matter of fact, our unpublished results indicated that DNA-PKcs was also down-regulated in cells with RPRM overexpression (Unpublished data).

In addition to enhancing cancer cell killing in cancer therapy, normal tissue must be protected against therapy-induced damage. However, until now radiation injury caused by radiotherapy and radiation accident remains a huge challenge. Short-lived free radicals produced by IR play a big role in radiation injury because of their damaging effects on cellular components especially DNA (Citrin et al., 2010). Therefore, free radicals are a common target for radiation protection. In fact, a majority of radioprotectors tested so far are antioxidants that scavenge free radicals thus alleviating cellular damage caused by IR (Citrin et al., 2010). However, despite extensive testing, to date there is only one radioprotector, i.e., amifostine, that was approved by FDA for clinical use, and its use is very limited because of its inconclusive protective effects in clinical trials, its side effects (nausea and hypotension) and delivery modality (it must be delivered prior to irradiation) (Citrin, 2019). This suggests that targets other than free radicals need to be explored to develop better and more effective radioprotectors. In this study, in addition to cancer cells, we further confirmed the determining role of RPRM in the radiosensitivity of normal cells and tissues. We found that RPRM-deficient cells were more resistant to IR than their WT counterparts. More intriguingly, RPRM-knockout mice exhibited delayed death after exposed to WBI and much less severe intestinal injury after exposed to WAI compared with WT mice. These results suggest that RPRM, a novel important DDR protein, may be also a potential target for radiation protection.

In summary, we discovered a novel critical role of RPRM in DNA repair and cellular sensitivity to DNA damage, and revealed an important underlying mechanism that RPRM translocates to the nucleus and interacts with ATM to promote the nuclear-cytoplasmic translocation of ATM resulting in its degradation and down-regulation, in which the phosphorylation of RPRM at serine 98 mediated by CDK4/6 is involved and IPO11 is required. These data not only shed light on the vital regulatory effect of RPRM on ATM, but also highlight the potential implications of RPRM in both cancer therapy and radiation protection.

Limitations of the study

Despite our important discoveries, there are some limitations in this study need to be pointed out. For example, we revealed that RPRM quickly translocated to the nucleus after induced by irradiation, interacted with ATM and promoted its nuclear export, but we did not give a clear explanation on some questions such as what exact role RPRM played in triggering ATM nuclear export, how ATM was exported from the nucleus. Besides, we found that both CDK4 and CDK6 could directly phosphorylate RPRM, but because of the lack of specific inhibitors, whether they played the same critical role in the nuclear translocation of RPRM was not elucidated. Although further investigation is warranted, the data we present here clearly demonstrated our finding that RPRM negatively regulates ATM levels through its nuclear translocation upon irradiation mediated by CDK4/6 and IPO11.

STAR★METHODS

Detailed methods are provided in the online version of this paper and include the following:

- KEY RESOURCES TABLE
- RESOURCE AVAILABILITY
  - Lead contact
  - Materials availability
  - Data and code availability
- EXPERIMENTAL MODEL AND SUBJECT DETAILS
  - Method details
- QUANTIFICATION AND STATISTICAL ANALYSIS

SUPPLEMENTAL INFORMATION

Supplemental information can be found online at https://doi.org/10.1016/j.isci.2022.105115.

ACKNOWLEDGMENTS

This work was supported by the National Natural Science Foundation of China (Grants U1632270 and U1967220) and the Priority Academic Program Development of Jiangsu Higher Education Institution (PARD).

AUTHOR CONTRIBUTIONS

Conceptualization: H. Y.; Validation: J. W. and J. C.; Formal analysis: Y.Z. and G.O; Investigation: Y.Z, G.O, Z.Y, Z.Z, Q.C., and M.L.; Writing: H.Y. and Y.Z.; Visualization: Y.Z. and G.O; Supervision: H.Y.; Project administration: H.Y., J.W., and J.C.; Funding acquisition: H.Y. and J.C.

DECLARATION OF INTERESTS

Except that Hongying Yang, Yarui Zhang, and Jingdong Wang are holding a Chinese patent entitled "An establishment of RPRM knockout mouse model and its implications" (Patent No: ZL 2019 1 0405248.9), the authors declare no competing interests.

INCLUSION AND DIVERSITY

We support inclusive, diverse, and equitable conduct of research.

Received: April 29, 2022
Revised: July 21, 2022
Accepted: September 8, 2022
Published: October 21, 2022

REFERENCES

Ahmed, M., Li, L., Pinnix, C., Dabaja, B., Nomie, K., Lam, L., and Wang, M. (2016). ATM mutation and radiosensitivity: an opportunity in the therapy of mantle cell lymphoma. Crit. Rev. Oncol. Hematol. *107*, 14–19.

Alexander, A., Cai, S.L., Kim, J., Nanez, A., Sahin, M., MacLean, K.H., Inoki, K., Guan, K.L., Shen, J., Person, M.D., et al. (2010). ATM signals to TSC2 in the cytoplasm to regulate mTORC1 in response to ROS. Proc. Natl. Acad. Sci. USA *107*, 4153–4158.

Amigo, J., Opazo, J., Jorquera, R., Wichmann, I., Garcia-Bloj, B., Alarcon, M., Owen, G., and Corvalán, A. (2018). The reprimo gene family: a novel gene lineage in gastric cancer with tumor suppressive properties. Int. J. Mol. Sci. *19*, 1862.

Anderson, L., Henderson, C., and Adachi, Y. (2001). Phosphorylation and rapid relocalization of 53BP1 to nuclear foci upon DNA damage. Mol. Cell Biol. *21*, 1719–1729.

Anheim, M., Tranchant, C., and Koenig, M. (2012). The autosomal recessive cerebellar ataxias. N. Engl. J. Med. *366*, 636–646.

Bakkenist, C.J., and Kastan, M.B. (2003). DNA damage activates ATM through intermolecular autophosphorylation and dimer dissociation. Nature *421*, 499–506.

Bech-Otschir, D., Kraft, R., Huang, X., Henklein, P., Kapelari, B., Pollmann, C., and Dubiel, W. (2001). COP9 signalosome-specifc phosphorylation targets p53 to degradation by the ubiquitin system. EMBO J. *20*, 1630–1639.

Bensimon, A., Schmidt, A., Ziv, Y., Elkon, R., Wang, S.Y., Chen, D.J., Aebersold, R., and Shiloh, Y. (2010). ATM-dependent and -independent dynamics of the nuclear phosphoproteome after DNA damage. Sci. Signal. *3*, rs3.

Berkovich, E., Monnat, R.J., and Kastan, M.B. (2007). Roles of ATM and NBS1 in chromatin structure modulation and DNA double-strand break repair. Nat. Cell Biol. *9*, 683–690.

Brooks, P., Fuertes, G., Murray, R.Z., Bose, S., Knecht, E., Rechsteiner, M.C., Hendil, K.B., Tanaka, K., Dyson, J., and Rivett, J. (2000). Subcellular localization of proteasomes and their regulatory complexes in mammalian cells. Biochem. J. *346 Pt 1*, 155–161.

Buchegger, K., Ili, C., Riquelme, I., Letelier, P., Corvalán, A.H., Brebi, P., Huang, T.H.M., and Roa, J.C. (2016). Reprimo as a modulator of cell migration and invasion in the MDA-MB-231 breast cancer cell line. Biol. Res. *49*, 5.

Buchegger, K., Riquelme, I., Viscarra, T., Ili, C., Brebi, P., Huang, T., and Roa, J. (2017). Reprimo, a potential p53-dependent tumor suppressor gene, is frequently hypermethylated in estrogen receptor α-positive breast cancer. Int. J. Mol. Sci. *18*, 1525.

Chen, M., Nowak, D.G., Narula, N., Robinson, B., Watrud, K., Ambrico, A., Herzka, T.M., Zeeman, M.E., Minderer, M., Zheng, W., et al. (2017). The nuclear transport receptor Importin-11 is a tumor suppressor that maintains PTEN protein. J. Cell Biol. *216*, 641–656.

Chook, Y.M., and Blobel, G. (2001). Karyopherins and nuclear import. Curr. Opin. Struct. Biol. *11*, 703–715.

Chun, H.H., and Gatti, R.A. (2004). Ataxia-telangiectasia, an evolving phenotype. DNA Repair *3*, 1187–1196.

Citrin, D.E. (2019). Radiation modifiers. Hematol. Oncol. Clin. North Am. *33*, 1041–1055.

Citrin, D., Cotrim, A.P., Hyodo, F., Baum, B.J., Krishna, M.C., and Mitchell, J.B. (2010). Radioprotectors and mitigators of radiation-induced normal tissue injury. Oncologist *15*, 360–371.

Daboussi, F., Dumay, A., Delacôte, F., and Lopez, B.S. (2002). DNA double-strand break repair signalling: the case of RAD51 post-translational regulation. Cell. Signal. *14*, 969–975.

Durant, S.T., Zheng, L., Wang, Y., Chen, K., Zhang, L., Zhang, T., Yang, Z., Riches, L., Trinidad, A.G., Fok, J.H.L., et al. (2018). The brain-penetrant clinical ATM inhibitor AZD1390 radiosensitizes and improves survival of preclinical brain tumor models. Sci. Adv. *4*, eaat1719.

Ewing, R.M., Chu, P., Elisma, F., Li, H., Taylor, P., Climie, S., McBroom-Cerajewski, L., Robinson, M.D., O'Connor, L., Li, M., et al. (2007). Large-scale mapping of human protein-protein interactions by mass spectrometry. Mol. Syst. Biol. *3*, 89.

Fernandez-Capetillo, O., Chen, H.T., Celeste, A., Ward, I., Romanienko, P.J., Morales, J.C., Naka, K., Xia, Z., Camerini-Otero, R.D., Motoyama, N., et al. (2002). DNA damage-induced G2-M checkpoint activation by histone H2AX and 53BP1. Nat. Cell Biol. *4*, 993–997.

Goldstein, M., and Kastan, M.B. (2015). The DNA damage response: implications for tumor responses to radiation and chemotherapy. Annu. Rev. Med. *66*, 129–143.

Görlich, D., and Kutay, U. (1999). Transport between the cell nucleus and the cytoplasm. Annu. Rev. Cell Dev. Biol. *15*, 607–660.

Göttgens, E.L., Bussink, J., Leszczynska, K.B., Peters, H., Span, P.N., and Hammond, E.M. (2019). Inhibition of CDK4/CDK6 enhances radiosensitivity of HPV negative head and neck squamous cell carcinomas. Int. J. Radiat. Oncol. Biol. Phys. *105*, 548–558.

Harbour, J.W., Luo, R.X., Dei Santi, A., Postigo, A.A., and Dean, D.C. (1999). Cdk phosphorylation triggers sequential intramolecular interactions that progressively block Rb functions as cells move through G1. Cell *98*, 859–869.

Hinz, M., Stilmann, M., Arslan, S.Ç., Khanna, K.K., Dittmar, G., and Scheidereit, C. (2010). A cytoplasmic ATM-TRAF6-cIAP1 module links nuclear DNA damage signaling to ubiquitin-mediated NF-κB activation. Mol. Cell *40*, 63–74.

Huang, C.Y., Hsieh, F.S., Wang, C.Y., Chen, L.J., Chang, S.S., Tsai, M.H., Hung, M.H., Kuo, C.W., Shih, C.T., Chao, T.I., et al. (2018). Palbociclib enhances radiosensitivity of hepatocellular carcinoma and cholangiocarcinoma via inhibiting ataxia telangiectasia-mutated kinase-mediated DNA damage response. Eur. J. Cancer *102*, 10–22.

Huttlin, E.L., Bruckner, R.J., Navarrete-Perea, J., Cannon, J.R., Baltier, K., Gebreab, F., Gygi, M.P., Thornock, A., Zarraga, G., Tam, S., et al. (2021). Dual proteome-scale networks reveal cell-specific remodeling of the human interactome. Cell *184*, 3022–3040.e28.

Jacquemin, V., Rieunier, G., Jacob, S., Bellanger, D., d'Enghien, C.D., Laugé, A., Stoppa-Lyonnet, D., and Stern, M.H. (2012). Underexpression and abnormal localization of ATM products in ataxia telangiectasia patients bearing ATM missense mutations. Eur. J. Hum. Genet. *20*, 305–312.

Jin, M.H., and Oh, D.Y. (2019). ATM in DNA repair in cancer. Pharmacol. Ther. *203*, 107391.

Karlin, J., Allen, J., Ahmad, S.F., Hughes, G., Sheridan, V., Odedra, R., Farrington, P., Cadogan, E.B., Riches, L.C., Garcia-Trinidad, A., et al. (2018). Orally bioavailable and blood-brain barrier-penetrating ATM inhibitor (AZ32) radiosensitizes intracranial gliomas in Mice. Mol. Cancer Ther. *17*, 1637–1647.

Kastan, M.B., and Lim, D.S. (2000). The many substrates and functions of ATM. Nat. Rev. Mol. Cell Biol. *1*, 179–186.

Kim, J.J., Lee, S.B., Yi, S.Y., Han, S.A., Kim, S.H., Lee, J.M., Tong, S.Y., Yin, P., Gao, B., Zhang, J., et al. (2017). WSB1 overcomes oncogene-induced senescence by targeting ATM for degradation. Cell Res. *27*, 274–293.

Kinner, A., Wu, W., Staudt, C., and Iliakis, G. (2008). γH2AX in recognition and signaling of DNA double-strand breaks in the context of chromatin. Nucleic Acids Res. *36*, 5678–5694.

Krejci, L., Altmannova, V., Spirek, M., and Zhao, X. (2012). Homologous recombination and its regulation. Nucleic Acids Res. *40*, 5795–5818.

Lavin, M.F. (2008). Ataxia-telangiectasia: from a rare disorder to a paradigm for cell signalling and cancer. Nat. Rev. Mol. Cell Biol. *9*, 759–769.

Lee, J.H., and Paull, T.T. (2004). Direct activation of the ATM protein kinase by the Mre11/Rad50/Nbs1 complex. Science *304*, 93–96.

Li, D., Tavana, O., Sun, S.C., and Gu, W. (2018). Peli1 modulates the subcellular localization and activity of Mdmx. Cancer Res. *78*, 2897–2910.

Marechal, A., and Zou, L. (2013). DNA damage sensing by the ATM and ATR kinases. Cold Spring Harb. Perspect. Biol. *5*, a012716.

Matsuoka, S., Ballif, B.A., Smogorzewska, A., McDonald, E.R., Hurov, K.E., Luo, J., Bakalarski, C.E., Zhao, Z., Solimini, N., Lerenthal, Y., et al. (2007). ATM and ATR substrate analysis reveals extensive protein networks responsive to DNA damage. Science *316*, 1160–1166.

Nachmias, B., Khan, D.H., Voisin, V., Mer, A.S., Thomas, G.E., Segev, N., St-Germain, J., Hurren, R., Gronda, M., Botham, A., et al. (2022). IPO11 regulates the nuclear import of BZW1/2 and is necessary for AML cells and stem cells. Leukemia *36*, 1283–1295. https://doi.org/10.1038/s41375-022-01513-4.

Nakamura, K., Sakai, W., Kawamoto, T., Bree, R.T., Lowndes, N.F., Takeda, S., and Taniguchi, Y. (2006). Genetic dissection of vertebrate 53BP1: a major role in non-homologous end joining of DNA double strand breaks. DNA Repair *5*, 741–749.

Ohki, R., Nemoto, J., Murasawa, H., Oda, E., Inazawa, J., Tanaka, N., and Taniguchi, T. (2000). Reprimo, a new candidate mediator of the p53-mediated cell cycle arrest at the G2 phase. J. Biol. Chem. *275*, 22627–22630.

Ooki, A., Yamashita, K., Yamaguchi, K., Mondal, A., Nishimiya, H., and Watanabe, M. (2013). DNA damage-inducible gene, reprimo functions as a tumor suppressor and is suppressed by promoter methylation in gastric cancer. Mol. Cancer Res. *11*, 1362–1374.

Perlman, S.L., Boder, E., Sedgewick, R.P., and Gatti, R.A. (2012). Ataxia-telangiectasia. Handb. Clin. Neurol. *103*, 307–332.

Pesch, A.M., Hirsh, N.H., Chandler, B.C., Michmerhuizen, A.R., Ritter, C.L., Androsiglio, M.P., Wilder-Romans, K., Liu, M., Gersch, C.L., Larios, J.M., et al. (2020). Short-term CDK4/6 Inhibition radiosensitizes estrogen receptor-positive breast cancers. Clin. Cancer Res. *26*, 6568–6580.

Riches, L.C., Trinidad, A.G., Hughes, G., Jones, G.N., Hughes, A.M., Thomason, A.G., Gavine, P., Cui, A., Ling, S., Stott, J., et al. (2019). Pharmacology of the ATM inhibitor AZD0156: potentiation of irradiation and olaparib responses pre-clinically. Mol. Cancer Ther. *20*, 1614–1626.

Saavedra, K., Valbuena, J., Olivares, W., Marchant, M.J., Rodríguez, A., Torres-Estay, V., Carrasco-Avino, G., Guzmán, L., Aguayo, F., Roa, J.C., et al. (2015). Loss of expression of reprimo, a p53-induced cell cycle arrest gene, correlates with invasive stage of tumor progression and p73 expression in gastric cancer. PLoS One *10*, e0125834.

Sato, N., Fukushima, N., Matsubayashi, H., Iacobuzio-Donahue, C.A., Yeo, C.J., and Goggins, M. (2006). Aberrant methylation of Reprimo correlates with genetic instability and predicts poor prognosis in pancreatic ductal adenocarcinoma. Cancer *107*, 251–257.

Savitsky, K., Bar-Shira, A., Gilad, S., Rotman, G., Ziv, Y., Vanagaite, L., Tagle, D.A., Smith, S., Uziel, T., Sfez, S., et al. (1995). A single ataxia telangiectasia gene with a product similar to P1-3 kinase. Science *268*, 1749–1753.

Shiloh, Y. (2003). ATM and related protein kinases: safeguarding genome integrity. Nat. Rev. Cancer *3*, 155–168.

Shiloh, Y., and Ziv, Y. (2013). The ATM protein kinase: regulating the cellular response to genotoxic stress, and more. Nat. Rev. Mol. Cell Biol. *14*, 197–210.

Spacey, S.D., Gatti, R.A., and Bebb, G. (2000). The molecular basis and clinical management of ataxia telangiectasia. Can. J. Neurol. Sci. *27*, 184–191.

Takao, N., Kato, H., Mori, R., Morrison, C., Sonada, E., Sun, X., Shimizu, H., Yoshioka, K., Takeda, S., and Yamamoto, K. (1999). Disruption of ATM in p53-null cells causes multiple functional abnormalities in cellular response to ionizing radiation. Oncogene *18*, 7002–7009.

Tang, X., Jang, S.W., Wang, X., Liu, Z., Bahr, S.M., Sun, S.Y., Brat, D., Gutmann, D.H., and Ye, K. (2007). Akt phosphorylation regulates the tumour-suppressor merlin through ubiquitination and degradation. Nat. Cell Biol. *9*, 1199–1207.

Tapodi, A., Bognar, Z., Szabo, C., Gallyas, F., Sumegi, B., and Hocsak, E. (2019). PARP inhibition induces Akt-mediated cytoprotective effects through the formation of a mitochondria-targeted phospho-ATM-NEMO-Akt-mTOR signalosome. Biochem. Pharmacol. *162*, 98–108.

Xu, M., Knox, A.J., Michaelis, K.A., Kiseljak-Vassiliades, K., Kleinschmidt-DeMasters, B.K., Lillehei, K.O., and Wierman, M.E. (2012). Reprimo (RPRM) is a novel tumor suppressor in pituitary tumors and regulates survival, proliferation, and tumorigenicity. Endocrinology *153*, 2963–2973.

Zhang, X.D., and Matunis, M.J. (2005). Ub in charge: regulating E2 enzyme nuclear import. Nat. Cell Biol. *7*, 12–14.

Zhang, T., Shen, Y., Chen, Y., Hsieh, J.T., and Kong, Z. (2015). The ATM inhibitor KU55933 sensitizes radioresistant bladder cancer cells with DAB2IP gene defect. Int. J. Radiat. Biol. *91*, 368–378.

STAR★METHODS

KEY RESOURCES TABLE

REAGENT or RESOURCE	SOURCE	IDENTIFIER
Antibodies		
HA (for IP)	Beyotime	Cat#AH158; RRID: AB_2895203
Mouse IgG (control IgG for IP)	Beyotime	Cat#A7028; RRID: AB_2909433
ATM	GeneTex	Cat#GTX70103; RRID: AB_368161
RPRM	GeneTex	Cat#GTX110976; RRID: AB_11173091
Phospho-ATM	Cell Signaling Technology	Cat#13050; RRID: AB_2798100
CDK4	Abcam	Cat#ab199728; RRID: AB_2920615
CDK6	Beyotime	Cat#AC256
IPO11	Bethyl	Cat#A304-811A-T
IPO11	Abcam	Cat#ab221615
Histone H3	GeneTex	Cat#GTX122148; RRID: AB_10633308
LMNB2	Beyotime	Cat#AF0219
β-actin	Beyotime	Cat#AA128; RRID: AB_2861213
GAPDH	Beyotime	Cat#AF1186; RRID: AB_2920889
Tubulin	Beyotime	Cat#AT819
Goat Anti-mouse IgG (H+L) HRP conjugated	Beyotime	Cat#A0216; RRID: AB_2860575
Goat Anti-rabbit IgG (H+L) HRP conjugated	Beyotime	Cat#A0208; RRID: AB_2892644
γ-H2AX	Abcam	Cat#ab22551; RRID: AB_447150
53BP1	Abcam	Cat#ab21083; RRID: AB_722496
RAD51	GeneTex	Cat#GTX100469; RRID: AB_1951602
Phospho-ATM (for IFC)	Sigma-Aldrich	Cat#SAB1413106
HA	Beyotime	Cat#AF0039
Goat Anti-mouse IgG (DyLight 488)	GeneTex	Cat#GTX213111-04
Goat Anti-rabbit IgG (DyLight 488)	GeneTex	Cat#GTX213110-04; RRID: AB_2887579
Goat Anti-mouse IgG (Cy3)	Affinity Biosciences	Cat#S0012; RRID: AB_2844799
Goat Anti-rabbit IgG (Cy3)	Affinity Biosciences	Cat#S0011; RRID: AB_2844800
Ki-67	GeneTex	Cat#GTX16667; RRID: AB_422351

(*Continued on next page*)

Continued

REAGENT or RESOURCE	SOURCE	IDENTIFIER
Cleaved Caspase-3	Cell Signaling Technology	Cat#9661T
Bacterial and virus strains		
pHBLV-U6-MSC-CMV for shRNA (NC/RPRM)	Hanbio	HH20180419CJB
pLenti-U6-spgRNA (NC/IPO11)-CMV	OBiO	HY80332
Chemicals, peptides, and recombinant proteins		
Cisplatin (CDDP)	Sigma	P4394-250mg
cOmplete ULTRA Tablets	Roche	05892791001
Cycloheximide (CHX)	Selleck Chemicals	S7418
DAPI	Beyotime	c1002
EvaGreen 2×qPCR MasterMix	Abm	MasterMix-R
Hygromycin	MESGEN	MG5561S
Leptomycin B (LMB)	Beyotime	S1726
LipofectamineTM 2000	Invitrogen	11668-019
MG132	Selleck	S2619
Palbociclib (Palb)	Selleck	S15791
Protein G-Agarose	Beyotime	P2055-2mL
Puromycin	Beyotime	ST551-50mg
Purified RPRM peptides (77–109)	ChinaPeptides	N/A
Purified recombinant CDK4	Origene	TP301156
Purified recombinant CDK6	Origene	TP327978
Critical commercial assays		
Commet assay kit	Trevigen®	4250-050-K
Deposited data		
TCGA-GBMLGG RNA-seq	TCGA	http://linkedomics.org/
TCGA-GBMLGG clinical data	TCGA	http://linkedomics.org/
Experimental models: Cell lines		
A549	Cell Bank of Chinese Academy of Sciences	TCHu150
AGS	Cell Bank of Chinese Academy of Sciences	TCHu232
H1299	Cell Bank of Chinese Academy of Sciences	TCHu160
H460	Cell Bank of Chinese Academy of Sciences	TCHu205
HaCaT	China Center for Type Culture Collection	GDC0106
MEFs	This paper	N/A
WS1	ATCC	CRL-1502
Experimental models: Organisms/strains		
BALB/c nude mice	Beijing Vital River Laboratory Animal Technology	N/A
$RPRM^{-/-}$ C57BL/6 mice	This paper	N/A
WT C57BL/6 mice	GemPharmatech	N/A
Oligonucleotides		
qPCR primers for human RPRM: Forward: 5′-CTGGCCCTGGGACAAAGAC-3′ Reverse: 5′-TCAAAACGGTGTCACGGATGT-3′	This paper	N/A
qPCR primers for human β-actin: Forward: 5′-AAAAGCCACCCCACTTCTCTCT-3′ Reverse: 5′-AATGCTATCACCTCCCCTGTGT-3′	This paper	N/A

(*Continued on next page*)

Continued

REAGENT or RESOURCE	SOURCE	IDENTIFIER
qPCR primers for human ATM: Forward: 5′-TGCAACAGGTCTTCCAGATG-3′ Reverse: 5′-CAAGAACACCACTTCGCTGA-3′	This paper	N/A
qPCR primers for mouse RPRM: Forward: 5′-TGCATTTCCAGCTGGGTCTT-3′ Reverse: 5′-GAGTCAAACGGTGTCACGGA-3′	This paper	N/A
qPCR primers for mouse GAPDH: Forward: 5′-TGACCACAGTCCATGCCATC-3′ Reverse: 5′-GACGGACACATTGGGGGTAG-3′	This paper	N/A
IPO11-targeting gRNAs: Sequence1: 5′-TGTTCTTCAGGTGTTAACAC-3′ Sequence2: 5′-AACATGGAATTGATCGCTAC-3′ Sequence3: 5′-CTTTGGATATAAATGTAAGG-3′	This paper	N/A
shRNA sequence (Table S1)	This paper	N/A
Recombinant DNA		
pCMV3-N-HA	This paper	N/A
pCMV3-RPRM-HA	This paper	N/A
pCMV3-RPRMS98A-HA	This paper	N/A
pCMV3-RPRMΔ79-109-HA	This paper	N/A
Dominant-negative IPO11 mutant	Sino Biological	HG13382-NF(m1)
Human IPO11	Sino Biological	HG13382-NF
Software and algorithms		
Image J	NIH	https://imagej.nih.gov/ij
Image ProPlus 6.0	Media Cybernetics	https://www.mediacy.com
Origin 2019	OriginLab	https://www.originlab.com
Other		
Sequence of RPRM peptide (amino acid from 77-109): N-GCNLLIKSEGMINFLVKDRRPSKEVEAVVVGPY-C	This paper	N/A

RESOURCE AVAILABILITY

Lead contact

Further information and requests for resources and reagents should be directed to and will be fulfilled by the lead contact, Hongying Yang (yanghongying@suda.edu.cn).

Materials availability

The information on the plasmids and RPRM gene knockout mouse line generated in this study are available from the lead contact.

Data and code availability

- All experimental data reported in this article will be shared by the lead contact on request.
- This article analyzed existing, publicly available data. The accession numbers for the datasets are listed in the key resources table.
- This article does not report original code.

EXPERIMENTAL MODEL AND SUBJECT DETAILS

Method details

Mouse experiments

All animal procedures were approved by the Ethics Committee of Soochow University. Soochow University Medical Experimental Animal Care Guidelines in accordance with the National Animal Ethical Policies of China were strictly adhered to in all animal experiments. We established RPRM$^{-/-}$ C57BL/6 mice, which were processed by GemPharmatech Co. Ltd. under commission. The WT C57BL/6 mice obtained during breeding were used as control. Male BALB/c nude mice (3–5 weeks) were purchased from the Experimental Animal Centre of Soochow University. All mice were specific pathogen free (SPF), and were kept in SPF animal facility of Soochow University Experimental Animal Centre. All mice were randomly divided into different experimental groups. For the survival experiment, RPRM$^{-/-}$ C57BL/6 mice and WT mice aged 3 months (n = 40/group, including both male and female) were irradiated with 9 Gy whole body X-irradiation (2.0 Gy/min, 320 kVp, X-RAD320ix, PXi). The body weights of mice were measured daily until their deaths. For radiation-induced intestinal injury, male RPRM$^{-/-}$ C57BL/6 mice and WT mice aged 3 months (n = 3/group) received 9 Gy of whole abdominal X-irradiation (WAI, 1.16 Gy/min, 160 kVp, RAD SOURCERS2000 X-ray machine). Mice were sacrificed on day 3.5 after WAI, and the small intestines were harvested and processed for immunohistochemistry and HE staining. For xenograft cancer experiment, H460-NC (1×10^6) and H460-RPRM (3×10^6) cells were subcutaneously injected into the right flank of BALB/c nude mice. Once reaching approximate 100 mm^3 in volume, the tumors were topically irradiated with 5 Gy X-rays (1.16 Gy/min, 160 kVp, RAD SOURCERS2000 X-ray machine). And the tumor growth was then monitored daily using caliper measuring. Tumor volumes were calculated as length × width^2/2. Mice were sacrificed when tumor volume reached 1000 ± 100 mm^3 or on day 30 after irradiation.

Cell lines, cell culture and reagents

H460, H1299 and SNU-1 cells were cultured in RPMI1640 containing 10% FBS, 2.5 g/L glucose, 1.5 g/L sodium bicarbonate, 1% sodium pyruvate solution and 1% penicillin-streptomycin. A549 and AGS cells were cultured in F12K with 10% FBS, 1% penicillin-streptomycin and 2.5 g/L sodium bicarbonate. WS1 human embryonic dermal fibroblasts and HaCaT human immortalized keratinocytes were cultured in DMEM medium with high glucose containing 10% FBS and 1% penicillin-streptomycin. All cell lines were tested negative for mycoplasma. MEFs were isolated as described previously (Kim et al., 2017). Briefly, mouse embryos were harvested at E13 and the internal organs were removed, then the embryo bodies were digested using 0.25% trypsin-EDTA for 30 min at 37°C, and neutralized with DMEM containing 10% FBS. The tissue homogenate was then filtered through 40 μm nylon cell strainer (Falcon) and centrifuged at 1000 rpm for 5 min, and the pellets were resuspended and cultured in completed DMEM. The MEFs used in this study were at passage 4 and 5.

Plasmids and stable transfection

The plasmids were transfected into cells using Lipofectamine™ 2000. The medium was replaced with fresh complete medium 6 h later. For stable transfection, cells were subcultured 48–72 h after transfection and were grown in selective medium containing 8 μg/mL puromycin. Single-cell clones were selected and multiplied in growth medium containing 4 μg/mL puromycin.

Lentiviral infection

7×10^5 cells were cultured in 1 mL medium containing viral supernatant in 6-well plates for 4 h at 37°C, and were added with 1 mL fresh medium and continued to culture for 24 h. Gene expression and cell viability were assessed at least 48 h post-infection. For colony selection, cells were plated in 96-well plate and grown in selective medium containing 8 μg/mL puromycin and 400 μg/mL hygromycin, and multiplied in growth medium containing 4 μg/mL puromycin and 200 μg/mL hygromycin. shRNA targeting RPRM sequences are listed in Table S1. CRISPR/Cas 9 system was used to knockout IPO11 with three gRNAs (key resources table).

Neutral comet assay

Cells were collected after irradiation and resuspended in cold PBS at a density of 1×10^5 cells/mL. 50 μL of cell suspension was combined with 500 μL of molten LMAgarose (Trevigen), and 50 μL of mixture was pipetted on CometSlide™ (Trevigen®) immediately according to the manufacture's instruction. In brief, slides were placed at 4°C in the dark for 10 min and then sequentially immersed in lysis solution and

1×neutral electrophoresis buffer for 1 h and 30 min, respectively, followed by electrophoresis at 17 V for 45 min at 4°C (Mini-Sub® Cell GT, BIO- RAD). Slides were transferred to DNA precipitation solution for 30 min at room temperature (RT). After immersion in 70% ethanol for 30 min, slides were dried at 37°C for 15 min. Then slides were stained in 1×SYBR® Gold (Thermo Fisher Scientific) staining solution for 30 min at RT in the dark. Slides were examined under a laser scanning confocal microscopes (FV2000, Olympus) with an excitation wavelength of 496 nm and an emission wavelength of 522 nm.

RNA extraction and real-time RT-PCR

Total RNA was isolated using TRIzol® Reagent and quantified by NanoDrop 2000c (Thermo). According to the manufacture's protocols, reverse transcription and real-time qPCR were performed using 5×All-In-One RT MasterMix and EvaGreen 2×qPCR MasterMix, respectively. The primer sequences (Invitrogen) used for quantitative RT-PCR are listed in key resources table.

Protein extraction, co-immunoprecipitation and western blotting

For total protein extraction, cells were lysed in RIPA containing protease inhibitors for 1 h on ice, then centrifuged at 16,000 g for 10 min at 4°C, and the supernatant was collected. For co-immunoprecipitation (co-IP), the supernatant was successively incubated with primary antibody of HA or ATM at 4°C overnight and protein G-Agarose at 4°C for 3 h. After washing 5 times with RIPA, co-purified proteins by IP were analyzed by western blotting. Nuclear and cytoplasmic protein extraction was performed as previously described (Li et al., 2018). For western blotting, after denature, protein extracts were separated on a 6%–12% SDS-PAGE gel and transferred to PVDF membrane. Following blocking with 5% bovine serum albumin (BSA) or 5% non-fat milk, the proteins of interest were probed by sequential incubation with primary antibodies at 4°C overnight and secondary antibodies at RT for 2 h, and detected on a FluorChem™ M System (Alpha) after treatment with ECL-plus.

Immunofluorescence staining

Cells on coverslips were fixed in 4% paraformaldehyde for 15 min at RT. After permeabilization and blocking, cells were sequentially incubated with primary antibodies at RT for 45 min (γ-H2AX, 53BP1, RAD51) or 4°C overnight (ATM, phospho-ATM and HA), and secondary antibodies at RT for 50–120 min, followed by counterstaining with 5 μg/mL DAPI at RT for 5 min. Cells were then imaged under an Olympus FV1200 confocal fluorescence microscope.

Colony formation assay

Cells were seeded in 60 mm dishes or 6-well plates at appropriate densities according to different radiation doses and cell lines. After irradiation cells were continuously cultured for 2 weeks, followed by fixation in methanol for 15 min at RT and staining with methylene Blue. The colonies containing at least 50 cells were counted, and the percentage of cell survival was calculated. Sensitization enhancement ratio (SER) was calculated as the ratio of the irradiation dose required for the control group to obtain 30% survival to the radiation dose required to obtain the same survival rate after overexpression of RPRM.

Micronucleus formation assay

Cells seeded on coverslips were irradiated, 24 h later, cells were fixed with fixative (methanol: acetic acid/3:1 in volume) for 15 min at RT, followed by staining with DAPI. Cells were examined under a Leica DM2000 microscope using a 40× objective lens. Nuclei with micronucleus were counted as positive, 1000 nuclei were examined for each sample.

Mass spectrum

Purified RPRM peptides (1 μg) were incubated with purified recombinant CDK4 (0.2 μg) and CDK6 proteins (0.2 μg), respectively (the sequence of RPRM peptide is listed in key resources table). The reaction products were resolved in SDS-PAGE gel and the gel slices including all proteins were excised. After gel digestion, LC-MS/MS analysis was performed at the JingJie PTM Biolab Co. Ltd. Proteome Discoverer 1.3 was used to process the MS/MS data. Trypsin/P was used as cleavage enzyme. For precursor and fragment ions, mass error was set to 10 ppm and 0.02 Da, respectively. High peptide confidence was selected and peptide ion score was set >20.

H&E and immunohistochemistry staining

Tumors and mouse intestines were fixed in 4% paraformaldehyde for at least 24 h and dehydrated by gradient ethanol solution. Paraffin-embedded tissue sections were deparaffinized and rehydrated followed by staining with hematoxylin for 10 min and eosin for 1 min. For immunohistochemistry, antigen retrieval was performed in sodium citrate solution (pH 6.0) for 20 min at 98°C after deparaffinization and rehydration. Then, the sections were blocked in 10% goat serum containing 1% BSA for 2 h at RT and sequentially incubated with primary antibodies at 4°C overnight and secondary antibody for 1 h at RT. After counterstained with hematoxylin, the sections were examined under a microscope (IX73, Olympus), and the images were analyzed using image J or Image-Pro Plus 6.0.

QUANTIFICATION AND STATISTICAL ANALYSIS

All statistical analysis was performed using Origin 2019 software. Data are presented as the average of 3 independent experiments ± standard error (SEM). Statistical significance was calculated using two-sample t-test or two-way ANOVA with Tukey's correction. Survival of mice and cancer patients was presented using Kaplan-Meier curves and significance was assessed using log-rank test. $p < 0.05$ was considered significantly different between groups.